NOAA Technical Memorandum NWS TDL-61

A SHEARED COORDINATE SYSTEM FOR STORM SURGE EQUATIONS OF MOTION WITH A MILDLY CURVED COAST

Techniques Development Laboratory
Silver Spring, Md.
July 1976

noaa NATIONAL OCEANIC AND ATMOSPHERIC ADMINISTRATION / National Weather Service

NOAA TECHNICAL MEMORANDA

National Weather Service, Techniques Development Laboratory Series

The primary purpose of the Techniques Development Laboratory of the Office of Systems Development is to translate increases of basic knowledge in meteorology and allied disciplines into improved operating techniques and procedures. To achieve this goal, the laboratory conducts applied research and development aimed at the improvement of diagnostic and prognostic methods for producing weather information. The laboratory performs studies both for the general improvement of prediction methodology used in the National Meteorological Service and for the more effective utilization of weather forecasts by the ultimate user.

NOAA Technical Memoranda in the National Weather Service Techniques Development Laboratory series facilitate rapid distribution of material that may be preliminary in nature and which may be published formally elsewhere at a later date. Publications 1 through 5 are in the former series, Weather Bureau Technical Notes (TN), Techniques Development Laboratory (TDL) Reports; publications 6 through 36 are in the former series, ESSA Technical Memoranda, Weather Bureau Technical Memoranda (WBTM). Beginning with TDL 37, publications are now part of the series NOAA Technical Memoranda, National Weather Service (NWS).

Publications listed below are available from the National Technical Information Service (NTIS), U.S. Department of Commerce, Sills Bldg., 5285 Port Royal Road, Springfield, Va. 22151. Prices vary for paper copy; $1.45 microfiche. Order by accession number, when given, in parentheses at end of each entry.

Weather Bureau Technical Notes

TN 10 TDL 1 Objective Prediction of Daily Surface Temperature. William H. Klein, Curtis W. Crockett, and Carlos R. Dunn, September 1965. (PB-168-590)

TN 11 TDL 2 Hurricane Cindy Galveston Bay Tides. N. A. Pore, A. T. Angelo, and J. G. Taylor, September 1965. (PB-168-608)

TN 29 TDL 3 Atmospheric Effects on Re-Entry Vehicle Dispersions. Karl R. Johannessen, December 1965. (PB-169-381)

TN 45 TDL 4 A Synoptic Climatology of Winter Precipitation From 700-mb. Lows for the Intermountain Areas of the West. Donald L. Jorgensen, William H. Klein, and August F. Korte, May 1966. (PB-170-635)

TN 47 TDL 5 Hemispheric Specification of Sea Level Pressure From Numerical 700-mb. Height Forecasts. William H. Klein and Billy M. Lewis, June 1966. (PB-173-091)

ESSA Technical Memoranda

WBTM TDL 6 A Fortran Program for the Calculation of Hourly Values of Astronomical Tide and Time and Height of High and Low Water. N. A. Pore and R. A. Cummings, January 1967. (PB-174-660)

WBTM TDL 7 Numerical Experiments Leading to the Design of Optimum Global Meteorological Networks. M. A. Alaka and Frank Lewis, February 1967. (PB-174-497)

WBTM TDL 8 An Experiment in the Use of the Balance Equation in the Tropics. M. A. Alaka, D. T. Rubsam, and G. E. Fisher, March 1967. (PB-174-501)

WBTM TDL 9 A Survey of Studies of Aerological Network Requirements. M. A. Alaka, June 1967. (PB-174-984)

WBTM TDL 10 Objective Determination of Sea Level Pressure From Upper Level Heights. William Klein, Frank Lewis, and John Stackpole, May 1967. (PB-179-949)

WBTM TDL 11 Short Range, Subsynoptic Surface Weather Prediction. H. R. Glahn and D. A. Lowry, July 1967. (PB-175-772)

WBTM TDL 12 Charts Giving Station Precipitation in the Plateau States From 700-Mb. Lows During Winter. Donald L. Jorgensen, August F. Korte, and James A. Bunce, Jr., October 1967. (PB-176-742)

WBTM TDL 13 Interim Report on Sea and Swell Forecasting. N. A. Pore and W. S. Richardson, December 1967. (PB-177-038)

WBTM TDL 14 Meteorological Analysis of 1964-65 ICAO Turbulence Data. DeVer Colson, October 1968. (PB-180-268)

WBTM TDL 15 Prediction of Temperature and Dew Point by Three-Dimensional Trajectories. Ronald M. Reap, October 1968. (PB-180-727)

WBTM TDL 16 Objective Visibility Forecasting Techniques Based on Surface and Tower Observations. Donald M. Gales, October 1968. (PB-180-479)

WBTM TDL 17 Second Interim Report on Sea and Swell Forecasting. N. A. Pore and W. S. Richardson, January 1969. (PB-182-273)

WBTM TDL 18 Conditional Probabilities of Precipitation Amounts in the Conterminous United States. Donald L. Jorgensen, William H. Klein, and Charles F. Roberts, March 1969. (PB-183-144)

WBTM TDL 19 An Operationally Oriented Small-Scale 500-Millibar Height Analysis Program. Harry R. Glahn and George W. Hollenbaugh, March 1969. (PB-184-111)

WBTM TDL 20 A Comparison of Two Methods of Reducing Truncation Error. Robert J. Bermowitz, May 1969. (PB-184-741)

WBTM TDL 21 Automatic Decoding of Hourly Weather Reports. George W. Hollenbaugh, Harry R. Glahn, and Dale A. Lowry, July 1969. (PB-185-806)

WBTM TDL 22 An Operationally Oriented Objective Analysis Program. Harry R. Glahn, George W. Hollenbaugh, and Dale A. Lowry, July 1969. (PB-186-129)

WBTM TDL 23 An Operational Subsynoptic Advection Model. Harry R. Glahn, Dale A. Lowry, and George W. Hollenbaugh, July 1969. (PB-186-389)

WBTM TDL 24 A Lake Erie Storm Surge Forecasting Technique. William S. Richardson and N. Arthur Pore, August 1969. (PB-185-778)

(Continued on inside back cover)

U.S. DEPARTMENT OF COMMERCE
National Oceanic and Atmospheric Administration
ENVIRONMENTAL DATA SERVICE
Washington, D.C. 20235

Date: August 20, 1976

To: All Holders of NOAA Technical Memorandum NWS TDL-61 entitled "A Sheared Coordinate System for Storm Surge Equations of Motion With a Mildly Curved Coast"

From: C. P. Jelesnianski

Subject: Errata in NOAA Technical Memorandum NWS TDL-61

p. 4 Figure 1, caption line 3 should read ".... in the transformation. η is the distance ...."

p. 9 footnote, line 1 should read "* $\vec{\tau} = C|\vec{W}|\vec{W}$, where $\vec{W}$ ...."

p. 10 footnote, line 2 should read "is most inconvenient for coastal ...."

p. 15 3rd equation in second column should read

$$B_3 = [(B_i)_{m,n} - (B_r)_{m,n}\, a_1]\, b_3.$$

p. 17 1st line on right side of equation (18) should read

$$B_1(V^*)^{k-1}_{1,n} - (B_2 {}^{L}D^{5}_{y^*} + B_3 {}^{\overline{L}}D^{5}_{x^*})(hD)^{k}_{1,n} + h^{k}_{1,n}(B_2 {}^{L}D^{5}_{y^*} + B_3 {}^{L}D^{5}_{x^*})D_{1,n}$$

numerator on right side of equation (19) should read

$$(A_2 {}^{\overline{L}}D^{5}_{x^*} - A_3 {}^{L}D^{5}_{y^*})(hD)^{k+1}_{1,n} - A_4(V^*)^{k+1}_{1,n} - A_6$$

p. 33 4th line from botton of page should read

"But Δ reaches its maximum ...."

NOAA Technical Memorandum NWS TDL-61

A SHEARED COORDINATE SYSTEM FOR STORM SURGE EQUATIONS OF MOTION WITH A MILDLY CURVED COAST

Chester P. Jelesnianski

Techniques Development Laboratory
Silver Spring, Md.
July 1976

UNITED STATES
DEPARTMENT OF COMMERCE
Elliot L. Richardson, Secretary

NATIONAL OCEANIC AND
ATMOSPHERIC ADMINISTRATION
Robert M. White, Administrator

National Weather
Service
George P. Cressman, Director

CONTENTS

Abstract 1

1. Introduction 1

2. Basins described with a sheared coordinate system 3

3. The equations of motion in a sheared coordinate system 7

4. An explicit finite-difference scheme for interior and boundary points 11

   A. Interior points 14
   B. Coastal boundary 15

      1. computations with uncentered forms 16
      2. computations by "Method of Characteristics" 17

   C. The deep water boundary 21
   D. Lateral boundaries 22
   E. Corner points 22

5. An example and comparison with an unsheared system 23

6. Summary and conclusions 28

Acknowledgments 30

References 30

Appendix A. Stability Criteria 32

Appendix B. Sheared Coordinates 35

Appendix C. Some Special Problems with Surge Models 40

   A. Comments on Model Calibration and Input Boundary Conditions for Bay/Estuary Models 40
   B. Some Comments on Initialization of Models 44
   C. Some Comments on Storm Models and Driving Forces in Basins 48
   D. Some Comments on Short Gravity-Wind Waves and Wave Set-Up 50

A SHEARED COORDINATE SYSTEM FOR STORM SURGE EQUATIONS OF MOTION WITH A MILDLY CURVED COAST

Chester P. Jelesnianski

Techniques Development Laboratory
National Weather Service, NOAA
Silver Spring, Md.

ABSTRACT. To improve numerical computations of coastal storm surges, a mildly curved coastline is shifted or sheared onto a straight "baseline". A surface plane, truncated from the ocean shelf and containing the curved coast as a boundary, is fitted with a curved, non-orthogonal grid. The plane with curved boundaries is then transformed via a sheared coordinate system onto an image rectangle. In the transformed system, the computational grid is cartesian, orthogonal, equally spaced, and the coast lies exactly on and not across a grid line. Linearized transport equations of motion for storm surges are modified to accommodate the sheared coordinate system.

A surge model, incorporating the sheared system, is now fully operational for 3000 mi. of United States coasts, from the Mexican-American border in the Gulf of Mexico to the east end of Long Island, New York. The model can run with curvilinear storm tracks, changing storm celerity along the track, and changing storm parameters such as intensity and size.

1. INTRODUCTION

This report describes revisions of an operational storm surge model, SPLASH (Special Program to List Amplitudes of Surges from Hurricanes). The model is designed to compute tropical* storm surges on the open coast; i.e., a virtual coast unbroken by bays, estuaries, sounds, intracoastal waterways, deltas, capes, spits, etc. The range of applicability lies on 3000 mi. of coastline from Port Isabel, Texas to the east end of Long Island.

A major revision to the model, a sheared coordinate system to partially account for curved coastlines, is discussed in some detail. An offshoot of the "Method of Characteristics" is used to test and compare coastal boundary computations with our present methods. Also, the explicit finite-difference form used, and a cursory stability analysis of it, are discussed.

---

* Not to be confused with extratropical.

The model has been partially documented in three publications, the mathematical technique, Jelesnianski (1967), and two operational techniques to run and interpret the results for forecasting purposes, Jelesnianski (1972, 1974). The mathematical techniques are adapted from Platzman (1963). Another publication, Jelesnianski and Taylor (1973), discusses the tropical storm model used to generate surges.

To apply the equations of motion via finite differencing, it is convenient to use an orthogonal, equally-spaced, cartesian grid, and to treat natural coastlines as fixed boundaries. There are difficulties with this approach, however, because points on such a grid do not lie on naturally curved coastlines.

Coastal curvature, of course, can be ignored by subjectively distorting ocean basins into rectangles with straightline coasts. This procedure is especially useful when dealing with tropical storms whose curvature is much larger than coastal curvature, and if the storm's track is near normal to the coast.

Some models use stair-step boundaries to represent curved coastlines on a cartesian grid; however, there can be objections to treatment of inside/outside corners of the steps. Such a scheme is appropriate to contemplate surges atop the undisturbed sea surface of the basin, but not necessarily on coastal boundaries.

In storm surge applications one is not interested in circulation patterns inside basins but rather in surges on the coast and inland encroachment of sea water. If one has a choice on where to distort basins, then it is better to do so, say, on deep water boundaries and not the shoreline. Coastal water levels are usually of more interest than seaward levels across basins; consequently in numerical computations, curved coastal boundaries need as natural a representation as the interior of basins. In this report we consider continuously curved coastlines, fixed in space, with small but still significant curvature with respect to storm curvature; i.e., we consider a limited and restricted coastal curvature.

A natural approach is to form an orthogonal, curvilinear, coordinate system bounding the real coastline. Such a transformation preserves angles but not areas. The transformed equations of motion contain a variable magnification factor (a Jacobian) to account for area changes in the transformation.

Our approach, however, is to use a simple shearing transformation. The surface of an ocean basin with curved boundaries is transformed into a rectangle, with grid points lying on the transformed coast. Because we insist on coasts that curve gently (relative to storm curvature), strongly curved, broken-coast features--bays, estuaries, capes, sounds, inlets, intracoastal waterways, barrier island, etc.--must be ignored.

Our non-conformal, oblique or sheared, coordinate transformation preserves areas but not angles. The equations of motion are transformed through a variable slope factor to account for angle changes in the transformation. The

system has a non-variable Jacobian; e.g., no new terms are added to the transformed equations of motion--however, some coefficients of existing terms are changed.

For operational use, oceanographic data such as coastal geometry and shelf bathymetry of basins are permanently stored in the model for instant recall. To compute surges along a particular coastline, input data consisting only of simple meteorological data during storm passage are required. The parameters can be determined by weather forecasters; whereas, for planning purposes, hypothetical ones can be assigned.

The model is not calibrated locally with storm and surge data, Appendix C. Instead, it is only verified locally. In only a few cases does storm data exist jointly with surge data. In any local area it is rare that such data exists for more than one event. In fact, in most cases there are no appropriate data. Also, an acceptable calibration in a local area for one event may not hold for other events (e.g., other storms that are weaker/stronger, bigger/smaller, faster/slower, etc.). We use a universal calibration* for existing data on 3000 mi. of coastline. Coefficient values in the equations of motion and storm model, for drag, slip, viscosity, etc., are set once and for all in the model. These are fitted so as to verify with existing data in a useful or acceptable manner.

No revisions of the shelf bathymetry or coastline are used to help force agreement between observed and computed surges in local areas. Revisions are made when errors (punching, etc.) are discovered or whenever it is felt that more geographical and basin detail is appropriate, but we make no ad-hoc revisions solely to force computed results to agree with observed data. To fit our imposed shoreline constraints, some revisions in geography have been made, usually at some distance from the basin center. Also, some smoothing of bottom topography was made to prevent aliasing from bottom features smaller than two grid widths.

This generalized approach does not give the elegant and precise results one can obtain when calibrating for a particular storm event in a local area; however, it does give useful results for all storms in a global or large area rather than a local area.

2. BASINS DESCRIBED WITH A SHEARED COORDINATE SYSTEM

If tropical storm surges are to be modeled numerically, then the horizontal scale of the surge precludes treating an entire ocean. Also, for deep waters off the continental shelf, an explicit finite-difference scheme with constant grid size imposes unacceptable time steps in computations. To form a tractable geometric system, we truncate a basin from the ocean consisting of a limited length coastline and the surrounding shelf region, but not the deep ocean waters. Certain formalities are discussed in this section to prepare an input basin for our surge model.

---

* See Jelesnianski (1972), pp. 26-29.

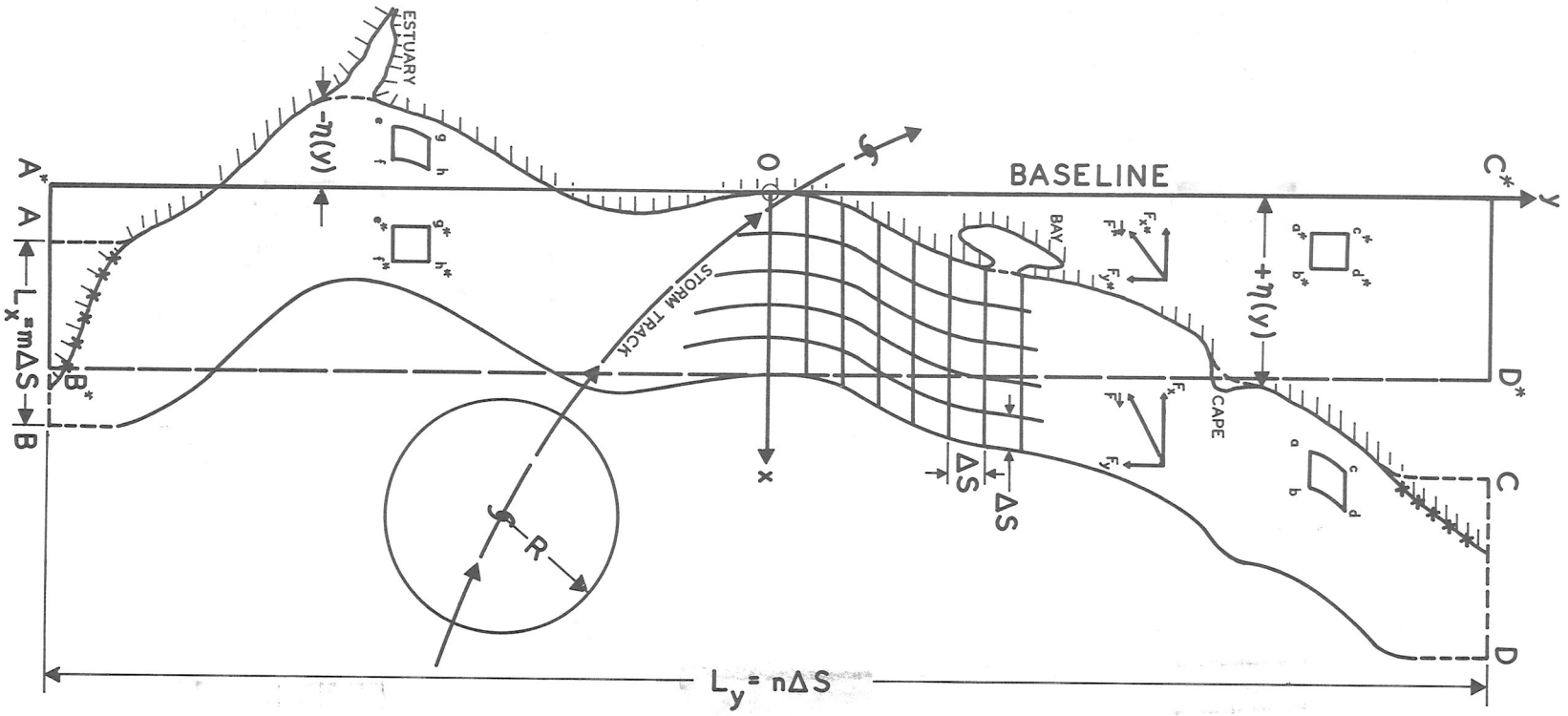

Figure 1.--A curved surface ABCD, truncated from the ocean shelf, is shifted or transformed into a rectangle "A*B*C*D*". The baseline, at its midpoint or basin center, is tangent to the coast at 0. Areas, but not angles, are conserved in the transformation. is the distance from the baseline to the coast as a function of y only. The quasi-curvilinear grid in ABCD becomes a cartesian, equally spaced grid in A*B*C*D*. Vectors, such as $\vec{F}$ or $\vec{F}^*$, have cartesian components in one system, but slanted or sheared components in the other system. R is the radius of maximum winds, and $R > \Delta s$. For further details, see the main text.

At a specified coastal point O, figure 1, consider the broad-scale features for the curved coastline, AOC (the coast about points A and C have been discarded to form convenient termini). All small-scale, broken-coast features--such as esturies, bays, capes, etc.--are discarded so that a general "open coast" boundary is formed. Curvature along this coast must be no larger than the curvature of tropical storms. One measure of curvature is the smallest R to be considered, where R, figure 1, is the distance from a storm's center to the radius of maximum winds. The grid spacing Δs should be small enough to see* a storm's curvature, and hence, curvature along a simulated coast. If $\Delta s \to R$, or if $\Delta s > R$, then there will be computational aliasing with finite-difference operators and the computed results are then suspect.

Draw a "baseline" on the y-axis of length L_y, bisected at the coastal point O. The length of L_y should be at least an order of magnitude larger than the largest R. The baseline (parallel to the y-axis) may be tangent to the coast as shown in the figure, but this is not necessary; in fact, when convenient, other orientations--subject to certain constraints--are admissable. Now consider the curve "BD", seaward and parallel to the coast "AC" at distance L_x from O; L_x is measured perpendicular from the baseline and its length** should be at least as large as the largest R or else the average width of the continental shelf. In a loose way, this second curve represents the junction of continental shelf and slope; it lies in deep water (<300 ft)*** and acts as an open boundary when boundary conditions are set. For computational convenience, the ends of the two parallel curves have been distorted to parallel the baseline; e.g., the coasts about points A and C have been discarded to form convenient termini. Now, connect the two parallel curves, AC and BD, with parallel, open-boundary lines AB and CD, perpendicular from the baseline. In this manner we construct a curvilinear parallelogram ABDC for the surface of a basin, with three open and one closed boundaries.

---

* Also, to see depth variations in the basin. If there are strong variations seaward, such as off the southeast Florida coast, then the grid distances must be small. One can "stretch" the coordinate system seaward so that grid points telescope toward the shore and elongate in deep water according to ocean depths; this is a project presently under development.

** This length is constant in our sheared coordinate system. One could, of course, use a stretching transformation to stretch this length according to shelf width (or bay/estuary width) with respect to the y-axis for a better description of basins. The mathematics are a bit more complicated; this remains as a project for the future.

*** If the depths are greater than 300 ft, they are arbitrarily set to 300 ft. Such a distortion in deep water has little effect on coastal waters during high surge activity.

An orthogonal, (x,y), rectangular grid on the surface of this basin would represent the curvilinear coast and deep water boundary in stair-step fashion. To eliminate the stair-steps, we form a quasi-curvilinear grid. On the curved surface ABDC, draw n lines perpendicular from the baseline, Δs apart, so the baseline length is $L_y = n\Delta s$; on the x-axis, draw m curves parallel to the coastline, Δs apart, so the shelf width is $L_x = m\Delta s$. This forms a non-orthogonal curvilinear grid of parallelograms with equal areas; for the particular curved net chosen, contra-variant base vectors span the space, Appendix B.

It is not desirable to compute with finite-difference forms using a non-orthogonal grid. Instead, we transform (strain) the basin ABDC onto the image rectangle A*B*D*C*; i.e., we shear the curvilinear grid. This is controlled by means of a shift function $\eta(y)$, which measures the perpendicular distance from the y-axis to the coast; each of the n horizontal lines of grid points on the curved parallelogram is shifted a distance $\eta(y)$ so that the coastal points fall on the y-axis (the baseline, of course, is then shifted an equal amount from the Oy axis). The area of ABDC is the same as A*B*D*C*; that is, shifting the curved parallelogram onto the linear parallelogram conserves areas. All parallelograms formed by the curvilinear grid, such as abdc or efhg are transformed or sheared onto squares, such as a*b*d*c* or e*f*h*g*. Thus we transform a non-orthogonal curvilinear grid, via the shift function $\eta(y)$, onto an orthogonal system. The transformed, sheared, or image orthogonal grid is now rectangular and labeled (x*,y*) so as not to confuse it with the original (x,y) coordinates; see figure 2.

Consider any vector $\vec{F}$ (such as wind, transport, forces, etc.) at a point on the basin's surface. It is represented in component form by two real numbers. For non-orthogonal frames, the two component numbers can have at least two different forms called contra-variant and co-variant, Appendix B. Any vector* may be represented in the computer by either variant form for the two component numbers or even in terms of components from an orthogonal frame. Of the three choices, it turns out that the mathematics are simplified (particularly the boundary conditions) if contra-variant component numbers are used.

The vector $\vec{F}$ in the original (x,y) coordinate system has components (F_x, F_y). Transforming the vector by means of the shift function $\eta(y)$ gives the sheared vector $\vec{F}^*$ on the image plane; it has components (F_{x^*}, F_{y^*}). The magnitude of $\vec{F}$ is changed by the transformation; e.g., the transformation conserves areas but not lengths.

The choice of new coordinate systems for the location of vectors and scalars and the choice of a new system of components imply that the dynamic equations must be re-written in terms of the new coordinates and components. This is done in the next section.

---

* In this report we will use vector components, magnitude of components, and component numbers interchangeably. For a description of contra-variant, co-variant, and other components, see Appendix B.

Although there are no boundary singularities such as inside/outside corners on stair-steps (except for the four corners on the termini of the basin), there are geometric restrictions of a practical nature applied to the basin and coast. The slope of the coast from the baseline can approach a right angle, but this is avoided. We arbitrarily restrict the slope to half a right angle ($\pi/4$ or 45^{o}) on either side of the baseline for a total slope change of 90^{o}; our motivation for this subjective restriction is governed by stability criteria of explicit finite-difference forms. It turns out that time steps in numerical computations are related inversely to $[1 + (d\eta/dy)^2]^{\frac{1}{2}}$, Appendix A, so the larger the slope function $d\eta/dy$ the smaller the time step; as the slope approaches a right angle, the time step approaches zero. Choosing the slope no greater than $\pm\pi/4$ means the slope function can decrease time steps by a factor of $(2)^{-\frac{1}{2}}$; this is one disadvantage of the sheared system.

Techniques to extract depth values at basin grid points require subjective decision processes. Questions raised are: How is bathymetry distorted about discarded capes, figure 1, or the basin itself when coastal slope exceeds $\pm\pi/4$; how is shelf bathymetry smoothed from randomly observed data on marine charts, etc.? Discussions on some of these techniques are given by Barrientos and Jelesnianski (1973).

The models, as presently developed, cannot be used below Port Isabel, Tex. nor above Long Island, N.Y. The revisions of this report have been incorporated in the SPLASH models, Jelesnianski (1972, 1974), for 3000 mi. of coastline. Storms and their tracks can be variant with time, and the storm need not landfall.

3. THE EQUATIONS OF MOTION IN A SHEARED COORDINATE SYSTEM

A geographical plane with orthogonal (x,y) axes, figure 2.a, is ordinarily used in surge computations. This cartesian system is oriented with respect to some baseline such as a north/south "y" axis, or an axis tangent to the coast at a given coastal point. The natural coastline meanders about the "y"-axis.

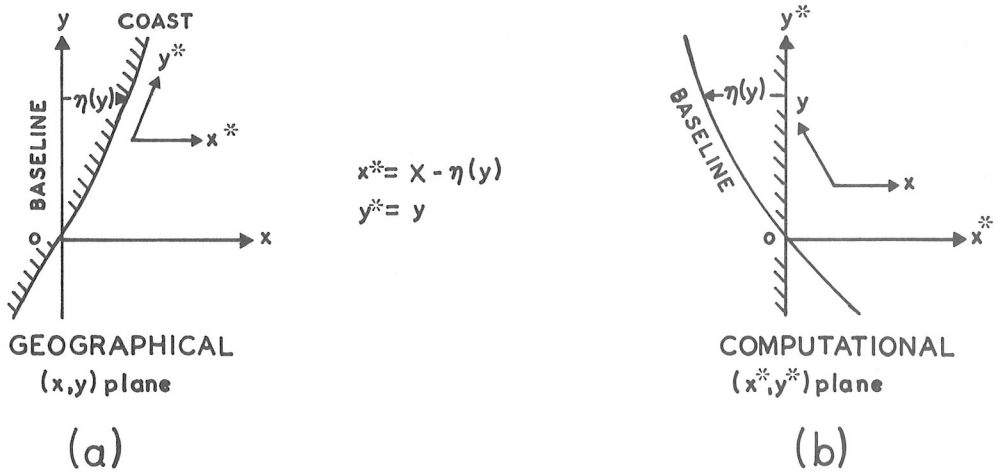

Figure 2.--(x,y) has cartesian components in the geographical plane, whereas (x^*, y^*) has sheared components. The opposite holds in the computational plane.

It is desirable to form a computational system whereby the coast is transformed into a straightline, figure 2.b; furthermore, we want this line to form one axis of an orthogonal, rectangular frame. This can be done with a simple shearing transformation through the shift function $\eta(y)$. The transformation shears the baseline into a curve and the natural coast into a straight line. In the computational or image plane, the original (x,y) axes are non-orthogonal, and the lengths are altered; similarly in the geographical or original plane, the image (x*,y*) axes are non-orthogonal and the lengths are altered. To use the computational (x*,y*) plane, consisting of a straightline coast perpendicular to the x*-axis, we must transform the surge equations of motion from the original geographical plane to the computational plane.

The storm surge equations of motion come in many forms and degrees of complexity. We limit the complexity in the SPLASH models because most users are interested in surges for a limited* period only; that is, on a coast, during the dominant stage of the forced wave under a storm. For this restriction, linearized equations of motion are suitable for forecasting purposes (the uncertainty of meteorological input parameters usually exceed non-linear effects). For extreme surges in shallow waters, the linearized model may overforecast the surge; the model is not designed to compute "probable maximum surges". Even with linearized equations, however, some complexities in surge dynamics need to be accounted for; these are unsteady flow from driving forces, its effects on bottom stress (time history bottom stress), and the coriolis parameter in an ocean basin.

There are solutions for the linearized equations of motion with "time-history-bottom-stress" in numerical form; examples are a truncated power series expansion, Platzman (1963), and a solution in intergral form, Jelesnianski (1970). We have chosen the former for the SPLASH models because of ease in computation, core storage requirements, and economics; the computed results from either solution do not differ greatly and both are suitable for forecasting purposes.

---

* The model was designed to give the space envelope of highest surges on the coast. It was not designed to give a complete "time-history" or duration of the coastal surge. By "time-history" or duration we mean surge against time at any coastal point. The model is initialized with a quiescent sea, at most 12-hr before landfall or else before nearest approach of a storm to basin center, and 6-hr thereafter for at most an 18-hr run. At any coastal point, the computed, time-history, surge profile is viable at time of maximum surge but defective at the earliest limb of the profile. Of course, the model can be redesigned to incorporate longer time runs or duration, and this has been done for special runs (figure 6 is a special run for 36-hr); for practical forecasting this is wasteful of computer resources because such long duration runs do not ordinarily affect the space envelope of highest surges.

The linearized storm surge equations of motion in a geographical plane, Platzman (1963), and modified by the addition of a slip coefficient, Jelesnianski (1967), are

$$\frac{\partial U}{\partial t} = - gD\left[B_r \frac{\partial (h-h_o)}{\partial x} - B_i \frac{\partial (h-h_o)}{\partial y}\right] + f(A_r V + A_i U) + C_r {}^{x}\tau - C_i {}^{y}\tau$$

(1)
$$\frac{\partial V}{\partial t} = - gD\left[B_r \frac{\partial (h-h_o)}{\partial y} + B_i \frac{\partial (h-h_o)}{\partial x}\right] - f(A_r U - A_i V) + C_r {}^{y}\tau + C_i {}^{x}\tau$$

$$\frac{\partial h}{\partial t} = -\frac{\partial U}{\partial x} - \frac{\partial V}{\partial y}$$

where

U,V = transport components
h = surface height (the storm surge)
h_o = hydrostatic heights due to atmospheric pressure
f = coriolis parameter
D = depths
g = gravity
$x\tau, y\tau$ = components of surface stress*
A_r ..... C_i = bottom stress functions varying with depth

These equations are for the geographical plane of figure 2.a, with orthogonal (x,y) axes. To transform the above for the computational or image plane, figure 2.b, consider the following transformation,

(2)
$$x^* = x - \eta(y)$$
$$y^* = y$$

where the shift function η is a function of y only. Any vector $\vec{F^*}=(F_{x^*},F_{y^*})$ in the computational system has components in the geographical system as

(3)
$$F_{x^*} = \frac{\partial x^*}{\partial x} F_x + \frac{\partial x^*}{\partial y} F_y = F_x - \frac{\partial \eta}{\partial y} F_y$$

$$F_{y^*} = \frac{\partial y^*}{\partial x} F_x + \frac{\partial y^*}{\partial y} F_y = F_y.$$

---

* $\vec{\tau} = C\,|W|\,\vec{W}$, where $\vec{W}$ is vector wind and the drag coefficient $C = 3X10^{-6}$. The bottom stress functions use an eddy viscosity $\nu = 0.25$ ft^2/s and a slip coefficient $s = 0.006$ ft/s, see Jelesnianski (1967).

These components are a contra-variant form*, Appendix B. In particular the transports of eq. (1), from eq. (3) are, after rearrangement,

$$(4) \qquad U = U^* + \eta_y V^*$$

$$V = V^* \qquad , \eta_y = \frac{\partial \eta}{\partial y}$$

where U*, V* are contra-variant component numbers of transport, Appendix B. The gradients of the fields in eq. (1) are given through eq. (2), via a chain rule as

$$(5) \qquad \frac{\partial}{\partial x} = \frac{\partial x^*}{\partial x}\frac{\partial}{\partial x^*} + \frac{\partial y^*}{\partial x}\frac{\partial}{\partial y^*} = \frac{\partial}{\partial x^*}$$

$$\frac{\partial}{\partial y} = \frac{\partial x^*}{\partial y}\frac{\partial}{\partial x^*} + \frac{\partial y^*}{\partial y}\frac{\partial}{\partial y^*} = \frac{\partial}{\partial y^*} - \eta_y \frac{\partial}{\partial x^*}$$

Applying eq. (4) and eq. (5) in eq. (1), separating the time derivative of U*, V* gives

$$\frac{\partial U^*}{\partial t} - f A_i U^* = -g D\left[B_r (1 + \eta_y^2) \frac{\partial h}{\partial x^*} - (B_i + B_r \eta_y) \frac{\partial h}{\partial y^*} \right] + fA_r \left[(1 + \eta_y^2) V^* + \eta_y U^* \right] + {}^{x}T - \eta_y {}^{y}T$$

$$(6) \qquad \frac{\partial V^*}{\partial t} - f A_i V^* = -g D\left[B_r \frac{\partial h}{\partial y^*} + (B_i - B_r \eta_y) \frac{\partial h}{\partial x^*} \right] - fA_r (U^* + \eta_y V^*) + {}^{y}T$$

$$\frac{\partial h}{\partial t} = - \frac{\partial U^*}{\partial x^*} - \frac{\partial V^*}{\partial y^*}$$

where

$$(7) \qquad {}^{x}T = B_r \frac{\partial h_o}{\partial x} - B_i \frac{\partial h_o}{\partial y} + C_r {}^{x}\tau - C_i {}^{y}\tau$$

$${}^{y}T = B_r \frac{\partial h_o}{\partial y} + B_i \frac{\partial h_o}{\partial x} + C_r {}^{y}\tau + C_i {}^{x}\tau$$

---

* This form is very convenient for boundary conditions; the co-variant form is most convenient for coastal boundaries, see Appendix B. Birchfield and Murty (1974) shear and stretch a coordinate system in two-dimensions, but use untrasformed vector components; some manuevering is required to form transports on the boundary.

The components of the driving forces eq. (7) are retained in the original, geometrical (x,y) system because of convenience in computations. The field values (transports, surges), and their gradients, are in the (x*,y*) computational system. The arrangement of the coriolis terms in eq. (6) are in anticipation of explicit finite-differencing techniques. Notice in particular, the invariant character of the continuity equations in both coordinate systems eq. (1) and eq. (6); this occurs because areas are conserved* when mapping from one system to the other.

4. AN EXPLICIT FINITE-DIFFERENCE SCHEME FOR INTERIOR AND BOUNDARY POINTS

In numerical computations of storm surges, we use an equally spaced, staggered grid of size Δs, figure 3. Any field value $F(x^*,y^*,t)$, such as transport, surge or forces, is labeled $F^k_{m,n} = F(m\Delta s, n\Delta s, k\Delta t)$ on the grid, where "m,n,k" are integers. Note, "m" and "n" are both even or both odd at each point of the space-staggered grid**; also, (m+n) or (m-n) are even integers.

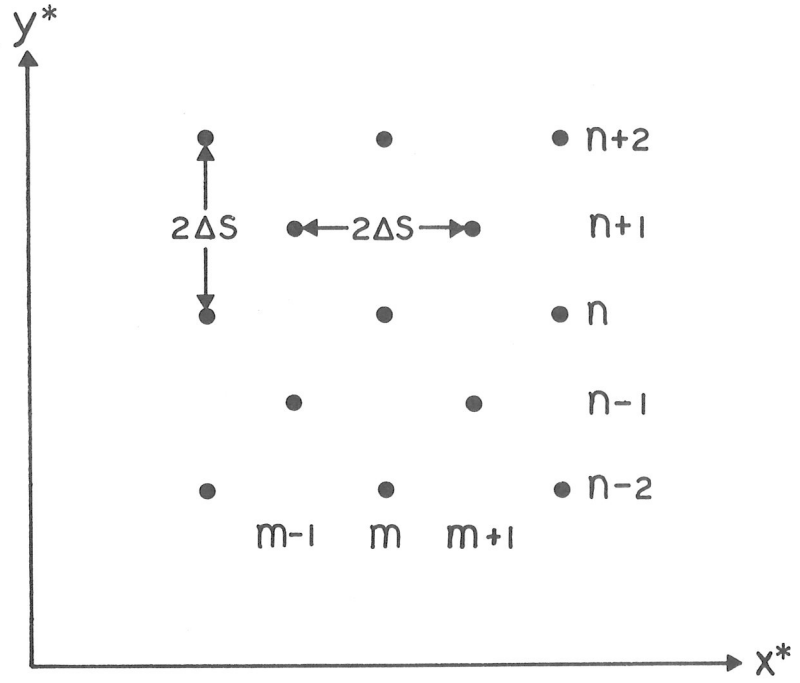

Figure 3.--An equally spaced, staggered grid in the (x*,y*) computational plane.

---

* We could shear and then stretch the coordinate system so that eq. (2) becomes $x^* = [\beta_o / \beta(y)]\,[x - \eta(y)]$, $y^* = y$, where β_o is a typical width along the x-axis and $\beta(y)$ is the width of the basin as a function of y. In this system, for a variable $\beta(y)$, areas are not conserved and the continuity equation is a bit more complicated. Note, shear and stretch are one-dimensional. Birchfield and Murty (1974) have made such an application for two-dimensional transforms.

** This is in contrast to the grid of figure 1 which is merely illustrative.

In our finite-difference scheme, we compute the three field values, "U*, V* and h", at every grid point. Compared to other schemes, the computer core storage for field values is excessive; for example, there are many ways to set up "leap-frog" schemes that use only half the core. Our scheme allows computations of surge values on boundaries. A better scheme could be designed to conserve core storage and still give the same information; this remains as a project for the future.

The equations of motion in differential form eq. (6) are

$$\frac{\partial U^*}{\partial t} = fA_i U^* - gD\left[B_r a_2 \frac{\partial h}{\partial x^*} - (B_i + B_r a_1)\frac{\partial h}{\partial y^*}\right] + fA_r(a_2 V^* + a_1 U^*) + {}^{x}_{T} - a_1 {}^{y}_{T}$$

(8)

$$\frac{\partial V^*}{\partial t} = fA_i V^* - gD\left[B_r \frac{\partial h}{\partial y^*} + (B_i - B_r a_1)\frac{\partial h}{\partial x^*}\right] - fA_r\,(U^* + a_1 V^*) + {}^{y}_{T}$$

$$\frac{\partial h}{\partial t} = -\frac{\partial U^*}{\partial x^*} - \frac{\partial V^*}{\partial y^*}$$

where $a_1 = \eta_y$, $a_2 = 1 + (a_1)^2$. In anticipation of finite differencing, we set $a_1 = (\eta_y)_n$, where "n" is shorthand for y* or y = n Δs. In this way we form discrete values for the coastal slope function $\eta_y = \frac{\partial \eta}{\partial y}$; note, the slope function varies only with "y".

For most of the United States coasts, the average offshore depths or slope at the coast is orders of magnitude larger than the slope a small distance seaward. Also, for a short distance inland, the coast is covered with dunes, figure 4. We have taken advantage of this geographical configuration by setting

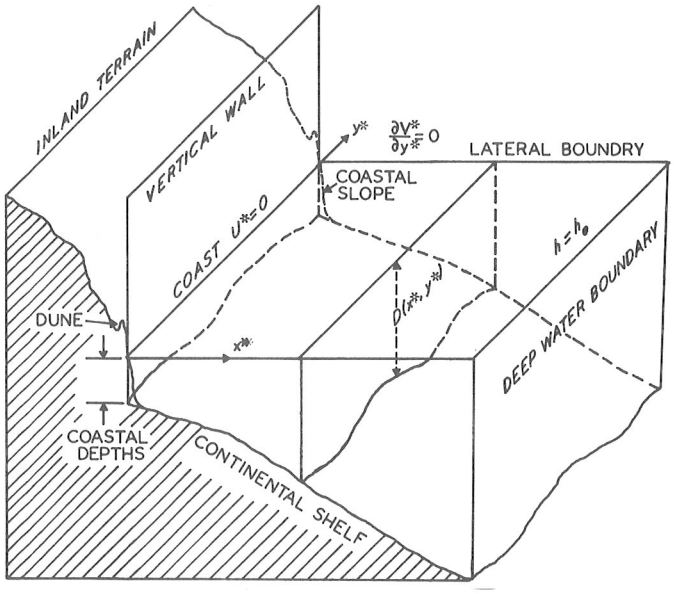

Figure 4.--The basin and boundary condition used in our model. A vertical wall simulates the rapidly changing land and ocean contours at the coast.

a vertical wall at the coast and extrapolating the local average shelf slope onto the vertical wall. In this way the undistrubed water depths of the United States coasts vary between 10-50 ft, with an average of about 15 ft. We also assume that the dunes are not overtopped, or if overtopped the distance of inundation inland is small compared to some scale length such as storm size. It is anticipated in future work, for inland inundation, this coastal configuration can be treated as a weir when dunes are overtopped.

Our truncated basin from the sea has three open and one coastal boundaries. The open boundaries do not have a physical boundary condition, but mathematically, boundary conditions are demanded. Hence, arbitrary conditions are set to approximate the influences of the exterior sea. There are three types of boundary conditions* used in our model:

1. On the coast, normal transport is zero but parallel transport is permitted. The coastal boundary is fixed in space. We are assuming a typical wavelength, for the storm surge wave, is much larger than any distance inland penetrated by seawater. This, of course, is not true for broken coast features such as bays and estuaries, or if the dunes are overtopped and the terrain for large distances inland is flat and even; in these cases, our boundary condition may overforecast the surge on the fixed coast.

2. The deep water, open boundary, uses static heights (the inverted barometer effect) of the storm.

3. Each lateral boundary (open boundary) has vanishing normal derivatives of transport. This is fictitious but convenient.

The basin, figure 1, is fictitious at and near lateral boundaries. We could consider an absorptive condition in regions surrounding the lateral boundaries; this remains as a future endeavor. We are assuming that surges at basin center, during storm passage when surges are extreme, are not affected by distant lateral boundaries; this is borne out with empirical tests for different sized basins.

In our finite-difference scheme, the time derivative is approximated as

$$(9) \qquad \frac{\partial F}{\partial t} = \frac{1}{2\,\Delta t}\left[F^{k+1}_{m,n} - F^{k-1}_{m,n} \right] .$$

For finite differencing of spatial derivatives, a notation for interior, boundary, and corner points will be developed.

---

* It can be shown that the boundary conditions are properly posed for the storm-surge, linear, differential equations of motion. Boundary conditions 2. and 3. reflect energy to the basin interior; however, bottom stress disipates some of the energy before it reaches the coast.

A. Interior Points

A five-point centered scheme is used for finite differencing of spatial derivatives. The "x*" derivative is approximated as

$$(10)\quad \frac{\partial F}{\partial x^*} = \frac{1}{4\,\Delta s}\left[F^k_{m+1,n+1} + F^k_{m+1,n-1} - F^k_{m-1,n+1} - F^k_{m-1,n-1}\right].$$

We now define an operator for the above, in positional form, as

$$(11a)\quad D^5_{x^*} = \begin{vmatrix} -1. & & 1. \\ & 0. & \\ -1. & & 1. \end{vmatrix}$$

Similarly, for the y* derivative,

$$(11b)\quad D^5_{y^*} = \begin{vmatrix} 1. & & -1. \\ & 0. & \\ -1. & & -1. \end{vmatrix}$$

Now let

$$b_1 = 2\,\Delta t$$
$$b_2 = \Delta t/2\,\Delta s$$
$$b_3 = g b_2$$

Then eq. (8) with eq. (9) and eq. (11), in finite-difference form, is

$$(U^*)^{k+1}_{m,n} = A_1(U^*)^{k-1}_{m,n} - D_{m,n}[A_2 D^5_{x^*} - A_3 D^5_{y^*}]h^k_{m,n} + \\ + A_4(V^*)^k_{m,n} + A_5(U^*)^k_{m,n} + A_6 {}^{x}T^k_{m,n} - A_7 {}^{y}T^k_{m,n}$$

$$(12)\quad (V^*)^{k+1}_{m,n} = B_1(V^*)^{k-1}_{m,n} - D_{m,n}[B_2 D^5_{y^*} + B_3 D^5_{x^*}]h^k_{m,n} - \\ - B_4(U^*)^k_{m,n} - B_5(V^*)^k_{m,n} + B_7 {}^{y}T^k_{m,n}$$

$$h^{k+1}_{m,n} = h^{k-1}_{m,n} - b_2[D^5_{x^*}(U^*)^k_{m,n} + D^5_{y^*}(V^*)^k_{m,n}]$$

where

$$A_1 = 1 + f(A_i)_{m,n} b_1 \qquad B_1 = A_1$$

$$A_2 = (B_r)_{m,n} a_2 b_3 \qquad B_2 = A_2/a_2$$

$$A_3 = [(B_i)_{m,n} + (B_r)_{m,n} a_1] b_3 \qquad B_3 = [(B_i)_{m,n} - (B_r)_{m,n} a_1 b_3$$

$$A_4 = f(A_r)_{m,n} a_2 b_1 \qquad B_4 = A_4/a_2$$

$$A_5 = A_4 a_1/a_2 \qquad B_5 = A_5$$

$$A_6 = b_1 \qquad B_6 = 0$$

$$A_7 = a_1 b_1 \qquad B_7 = b_1$$

Note the "past" times of transport associated with A_1, B_1 terms; this is a requirement for stability in the finite-difference scheme. A positional derivitive, such as "$D_x^5 * h_{m,n}^k$" means an operation through eq. (11), at time "k", centered at position (m,n), on any field. The friction coefficients, A_i, A_r, ..., have discrete values, $(A_i)_{m,n}$,....., at each grid point according to the depth $D_{m,n}$; these can be set initially once and for all (similarly for η_y) for each basin.

Under ideal conditions of constant depths, no bottom stress, and no driving forces, the stability criterion for eq. (12) is, Appendix A,

$$\Delta t \leq \frac{\Delta s}{\sqrt{gD\,[1 + (\eta_y^2)\,] + (f\Delta s)^2}} \tag{13}$$

Notice that if $|\eta_y|$ becomes too large, then Δt approaches zero; in our computations we conveniently restrict $|\eta_y| \leq 1$, or a slope of 45°. It turns out in practice that a " Δt" smaller than eq. (13) is required to ensure well-behaved solutions with boundaries. This is derived by empirical tests; usually a factor of $(2)^{-\frac{1}{2}}$ suffices.

The grid spacing in the present SPLASH models is 4 statute mi. Inasmuch as depths are not permitted to exceed 300 ft, then to maintain stability " Δt" is not quite 3 min. The models use a time increment of 120 sec.

B. Coastal Boundary

For coastal computations with the boundary condition U*=0, Appendix B, we discuss two methods to compute surges on the coastal boundary. The first method, which uses uncentered finite-difference forms in space, does not directly satisfy the continuity equation on the coast; it appears however, mass may be conserved about the coast. The truth of this assertion requires an extensive

exploration of uncentered finite-difference forms in space, and weights to be assigned to surrounding grid points; this remains as a project for the future. The second method, an offshoot of the "Method of Characteristics", does satisfy the continuity equation along the coast. If both methods are to apply, then it is necessary they compute equally well at the coast. Such equality however, does not guarantee that mass is conserved about a coast; a deeper study on this point is a project for the future.

For a linear system, with partial differential equations of motion and properly posed boundary conditions, there exists a unique solution for a given storm. However, a stable numerical solution is no guarantee of equivalency to the unique solution. We make no attempt to prove existence or uniqueness in our methods, and our approaches are empirical and intuitive.

1. Computations With Uncentered Forms

On this boundary normal transports are zero, and then the derivative with respect to time is also zero. In the absence of overtopping, a necessary condition on the boundary is that "drift" transport balances "slope" transport, (Jelesnianski 1970). To produce this balance we use the first momentum equation of eq. (8) with $\partial U^*/\partial t=0$. The spatial derivatives, in finite-difference form, allows one to extrapolate height values onto the coast to satisfy known terms in the equation.

Notice, we do not directly satisfy continuity on the coast. It is impossible to satisfy the three equations of eq. (8), in finite-difference form, plus the boundary condition, by direct means*; instead, we dispense with the continuity equation on the coastal boundary and rely on the momentum equations as being adequate for forecasting purposes. One can set complicated compatability requirements to satisfy all of eq. (8) and the boundary condition on the coast, but this remains as a project for the future.

On the boundary we use an uncentered form, which for the x* derivative is approximated as

$$(14) \qquad \frac{\partial F}{\partial x^*} = \frac{1}{4\,\Delta s}\left[-6F^k_{1,n} + 4(F^k_{2,n+1} + F^k_{2,n-1}) - F^k_{3,n+2} - F^k_{3,n-2}\right].$$

We now define positional operators on the coast as

$$(15) \qquad L_{D^5_{x^*}} = \begin{vmatrix} 0. & -1. \\ & 4. \\ -6. & 0. \\ & 4. \\ 0. & -1. \end{vmatrix} \quad , \quad L_{D^5_{y^*}} = \begin{vmatrix} 0. & -1. \\ & 4. \\ 0. & 0. \\ & -4. \\ 0. & 1. \end{vmatrix}$$

where "L" means left boundary on the rectangular grid, figure 1.

* One can use the "Method of Characteristics" to satisfy the equations and boundary condition. This is done in the following section, as a check on the procedures of this section.

By empirical means, we have found for variable depths that an expansion of the depth and surge gradients are desirable in boundary computations as

$$(16)\qquad D\frac{\partial h}{\partial x^*} = \frac{\partial (hD)}{\partial x^*} - h\frac{\partial D}{\partial x^*};\quad D\frac{\partial h}{\partial y^*} = \frac{\partial (hD)}{\partial y^*} - h\frac{\partial D}{\partial y^*}.$$

The above form permits numerical computations, if the sloping depths have zero depth at the coast. Empirically, we have found only small changes in surges if the bottom stress coefficients in eq. (12) are similarly expanded as in eq. (16). If we approximate eq. (16) by means of eq. (15), then the grid point with a factor of "6" becomes "0". Hence, we define a new positional operator for the left boundary on the coast as

$$(17)\qquad \bar{L}_{D^5_{x^*}} = \begin{vmatrix} 0. & -1. \\ & 4. \\ 0. & 0. \\ & 4. \\ 0. & -1. \end{vmatrix}.$$

Note, factor "6" does not appear in the y* derivative in eq. (15).

To compute the V* transports on the coast, the 2d momentum equation of eq. (12) is used, but with spatial derivatives incorporating eq. (16), (15), and (17), as

$$(18)\quad (V^*)^{k+1}_{1,n} = A_1(V^*)^{k-1}_{1,n} - (B_2 L_{D^5_{y^*}} + B_3 \bar{L}_{D^5_{x^*}})(hD)^k_{1,n} + h^k_{1,n}(B_2 L_{D^5_{y^*}} + B_3 \bar{L}_{D^5_{x^*}})D_{2,n}$$
$$- B_5(V^*)^k_{1,n} + B_7 {}^{y}T^k_{1,n}$$

where the subscripts (1,n) mean a point on the coastal boundary. Note: V* is not the orthogonal projection of the vector V on the coast. The transport component, projected parallel or tangent to the coast, is

$$V_{tngnt} = [\,\eta_y U^* + (1+\eta_y^2)V^*\,]\,/(1+\eta_y^2)^{\frac{1}{2}};$$

Similarly, $V_{normal} = U^*/(1+\eta_y^2)^{\frac{1}{2}}$, see Appendix B.

To compute heights on the coast, the 1st momentum equation of (12) is used, with U* and $\partial U^*/\partial t$ set to zero, and with spatial derivatives incorporating eq. (16), (15), and (17) as

$$(19)\qquad h^{k+1}_{1,n} = \frac{(A_2 \bar{L}_{D^5_{x^*}} - A_3 L_{D^5_{y^*}})(hD)^{k+1}_{1,n} - A_5(U^*)^{k+1}_{1,n} - A_6 {}^{x}T^{k+1}_{1,n} + A_7 {}^{y}T^{k+1}_{1,n}}{(A_2 \bar{L}_{D^5_{x^*}} - A_3 L_{D^5_{y^*}})D_{1,n}}$$

2. Computations by "Method of Characteristics"

We want to check the technique of the last section by comparing results with an alternate technique, an offshoot of the "Method of Characteristics". To develop the equations for this method requires some maneuvering. To begin,

consider the continuity and first momentum equation of eq. (18)

$$(20)\qquad \frac{\partial U^*}{\partial t} + gD\mathcal{A}\frac{\partial h}{\partial x^*} = gD\mathcal{B}\frac{\partial h}{\partial y^*} + \mathcal{C}V^* + \mathcal{D}U^* + {}^{x}F^*$$

$$\frac{\partial h}{\partial t} + \frac{\partial U^*}{\partial x^*} = -\frac{\partial V^*}{\partial y^*}$$

where $\mathcal{A} = B_r a_2$, $\mathcal{B} = B_r a_1 + B_i$, $\mathcal{C} = fA_r a_2$, $\mathcal{D} = f(A_r a_1 + A_i)$, ${}^{x}F^* = {}^{x}T - a_1 {}^{y}T$.

The above can be rewritten as

$$\frac{\partial U^*}{\partial t} + \sqrt{gD\mathcal{A}}\,\frac{\partial h\sqrt{gD\mathcal{A}}}{\partial x^*} = \sqrt{gD\mathcal{A}}\,h\,\frac{\partial\sqrt{gD\mathcal{A}}}{\partial x^*} + gD\mathcal{B}\frac{\partial h}{\partial y^*} + \mathcal{C}V^* + \mathcal{D}U^* + {}^{x}F^*$$

$$(21)\qquad \frac{\partial h\sqrt{gD\mathcal{A}}}{\partial t} + \sqrt{gD\mathcal{A}}\,\frac{\partial U^*}{\partial x^*} = -\sqrt{gD\mathcal{A}}\,\frac{\partial V^*}{\partial y^*}\,.$$

Now adding and subtracting these equations gives

$$\frac{\partial(U^* \pm h\sqrt{gD\mathcal{A}})}{\partial t} \pm \sqrt{gD\mathcal{A}}\,\frac{\partial(U^* \pm h\sqrt{gD\mathcal{A}})}{\partial x^*} = \sqrt{gD\mathcal{A}}\,h\,\frac{\partial\sqrt{gd\mathcal{A}}}{\partial x^*} + \mathcal{E} + \mathcal{D}U^*$$

where

$$\mathcal{E} = \mp\sqrt{gD\mathcal{A}}\,\frac{\partial V^*}{\partial y^*} + gD\mathcal{B}\frac{\partial h}{\partial y^*} + \mathcal{C}V^* + {}^{x}F^*$$

The previous equation can be written as

$$(22)\qquad \frac{D(U^* \pm h\sqrt{gD\mathcal{A}})}{Dt} = \sqrt{gD\mathcal{A}}\,h\,\frac{\partial\sqrt{gD\mathcal{A}}}{\partial x^*} + \mathcal{E} + \mathcal{D}U^*.$$

Some of the derivatives of the dynamic variables V*, h are kept in the $\mathcal{E}$ term and not combined in D/Dt. This reduces the full effectiveness of the method of characteristics in two-dimensions when all derivatives are combined into a differential operator in one direction (the characteristic direction). Hence the approach of this section is not a full fledged generalization; it only constitutes an extrapolation of the method of characteristics to three-dimensions.

Equation (23)has the characteristics*

$$(23) \quad dx^*/dt = \pm \sqrt{gD\mathcal{A}}$$

Notice, (x^*,t) are treated as variables in the substantive derivative of eq. (22), and the two equations of (21) telescope into one along a characteristic eq. (23). On the coastal boundary of a basin, eq. (22) holds on the negative characteristic; see figure 5. Hence, to predict at point P we need to know

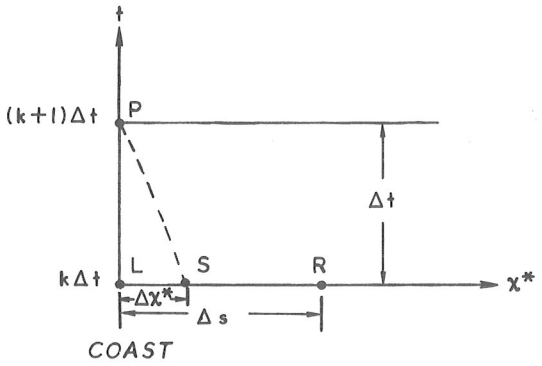

Figure 5.--An (x^*,t) system for the characteristic $dx^*/dt = -\sqrt{gd\mathcal{A}}$, see eq. (23). At time Δt, the characteristic must issue from point S on the abscissa so as to arrive at point P (the coast) at time $(k+1)\ \Delta t$. Δs is a grid length, and Δt is a computational time step.

all fields on the line LR, and in particular, on the point S at distance Δx^* from the coast; that is, the starting point on LR of the negative characteristic that intersects the coastal boundary at point P.

Once Δx^* is determined, then field values at point S can be interpolated from known values at discrete grid points such as L and R. We manipulate eq. (23) to form Δx^* as follows:

$$\Delta t = \int_L^S dx^* / \sqrt{gD\mathcal{A}}.$$

But the depths "D" and the coefficient $\mathcal{A}$ are almost linear along the line LR or LS. If the coast is set at $x^*=0$, and $gD\mathcal{A}$ is linearized, then

---

* We are assuming $\sqrt{gD\mathcal{A}}$ is a function of x^*; this holds about the coast where depths are small and the characteristic length between time steps is also small, where coastal curvature is small, and where depth changes dominate along the x^* coordinate. Should depths be deep and vary significantly along the y^* coordinate, and if coastal curvature is large, then eq. (23) does not hold and one must then consider curving bi-characteristics.

The methods of this section may not be applicable if one wishes to consider bay/estuary mouths, where depths vary significantly along both x^* and y^* coordinates, the coast curves dramatically, and flow axis through the mouth has a localized direction.

(24) $$\Delta t = \frac{1}{\sqrt{g}} \int_0^{\Delta x^*} dx^* / (a + bx^*)^{\frac{1}{2}} = \frac{2}{b\sqrt{g}} \left[(a + b\,\Delta x^*)^{\frac{1}{2}} - a^{\frac{1}{2}} \right]$$

where

$$a = (D\mathcal{A})_L, \quad b = \frac{[(D\mathcal{A})_R - (D\mathcal{A})_L]}{\Delta s}$$

and the subscripts L and R signify values at those points. Solving eq. (24) for Δx^* gives

(25) $$\Delta x^* = \Delta t \left[(gd\mathcal{A})_L^{\frac{1}{2}} + \frac{\Delta t}{4\,\Delta s} \{ (gD\mathcal{A})_R - (gD\mathcal{A})_L \} \right].$$

To interpolate any field value F at point S, we have chosen the following linear form,

(26) $$F_S = F_L + \frac{\Delta x^*}{\Delta s} (F_R - F_L).$$

Integrating eq. (22) on the characteristic, $dx^*/dt = -\sqrt{gD\mathcal{A}}$, gives

(27) $$(U^* - h\sqrt{gD\mathcal{A}})_P - (U^* - h\sqrt{gD\mathcal{A}})_S = \frac{\Delta t}{2} \left[\{ \sqrt{gD\mathcal{A}}\, h \frac{\partial \sqrt{gD\mathcal{A}}}{\partial x^*} + \mathcal{E} + \mathcal{D} U^* \}_P + \{ \sqrt{gD\mathcal{A}}\, h \frac{\partial \sqrt{gD\mathcal{A}}}{\partial x^*} + \mathcal{E} + \mathcal{D} U^* \}_S \right].$$

The coastal boundary condition, $U^*_P = U^*_L = 0$, gives

(28) $$h_P = \frac{-(U^* - h\sqrt{gD\mathcal{A}})_S - \frac{\Delta t}{2} \left[\{\mathcal{E}\}_P + \{ \sqrt{gD\mathcal{A}}\, h \frac{\partial \sqrt{gD\mathcal{A}}}{\partial x^*} + \mathcal{E} + \mathcal{D} U^* \}_S \right]}{\left[\sqrt{gD\mathcal{A}} \left(1 + \frac{\Delta t}{2} \frac{\partial \sqrt{gD\mathcal{A}}}{\partial x^*} \right) \right]_P}.$$

All fields, at point S, are determined from eq. (26), and includes U^*_S by setting $U^*_L = 0$. All field values at point R are mean values from the staggered grid; i.e., $U^*_R(\Delta s, n\Delta s, k\Delta t) = \frac{1}{2} U^*(\Delta s, (n+1)\Delta s, k\Delta t) + U^*(\Delta s, (n-1)\Delta s, k\Delta)$. The transport V^*_P is determined by the second momentum equation (8), and eq. (18). Derivatives, such as $\partial V^*/\partial y^*$ at point P and L, are determined by an uncentered form eq. (15); at point "R", by $\partial V^*/\partial y^* = \frac{1}{2\Delta s} V^*(\Delta s, (n+1)\Delta s, k\Delta t) - V^*(\Delta s, (n-1)\Delta s, k\Delta t)$.

There are ways, other than eq. (25) thru (27), to determine Δx^*, interpolation procedures for fields at point S, and approximate integration along a characteristic. After some empirical testing, we have chosen these methods because of their simplicity and performance. Results, with the techniques of this and the previous section, do not differ significantly. We have tested the two techniques for a range of storm conditions and basins normally encountered along the United States coasts. We have not tested for abnormal situations; i.e., very small storm sizes, extremely shallow/steep slopes on the continental shelf, etc.

C. The Deep Water Boundary

On this boundary, the heights are static from the "inverted barometer effect"; that is, the storm itself supplies height values on the boundary.

It is impossible to satisfy the three equations of (8) in finite-difference form, plus the boundary condition, by direct means*; instead, we dispense with the continuity equation on the deep water boundary and rely on the momentum equations as being adequate for forecasting purposes. One can set complicated compatibility requirements to satisfy all of eq. (8) and the boundary condition on the deep water boundary, but this remains as a project for the future; also a radiation type boundary condition may prove useful.

We define an uncentered positional operator on the coast which is eq. (15) rotated through 180°, with proper signs as

(29)
$$R_{D_{x^*}}^{5} = \begin{vmatrix} 1. & & 0. \\ & -4. & \\ 0. & & 6. \\ & -4. & \\ 1. & & 0. \end{vmatrix} \qquad R_{D_{y^*}}^{5} = \begin{vmatrix} -1. & & 0. \\ & 4. & \\ 0. & & 0. \\ & -4. & \\ 1. & & 0. \end{vmatrix}$$

where R means right boundary on the rectangular grid, figure 1. Also, as in eq. (17)

(30)
$$\bar{R}_{D_{x^*}}^{5} = \begin{vmatrix} 1. & & 0. \\ & -4. & \\ 0. & & 0. \\ & -4. & \\ 1. & & 0. \end{vmatrix} .$$

The transports are computed from the two momentum equations of (12) but with the spatial derivatives incorporating eq. (29), by eq. (16) and (30). The form is equivalent to eq. (18) for V*; similarly for the U* term.

The storm already provides static height gradients along the boundary if eq. (7) is rearranged in (x*,y*) coordinates, but in eq. (8) the dynamic height gradient is calculated by finite-difference forms. The static and dynamic height gradients along the boundary do not automatically cancel because the methods of calculation are different. For a sheared grid, empirical tests imply that is is better to explicitly compute the dynamic height gradient

---

* One can use "Method of Characteristics" to satisfy the equations and boundary condition. This is a project for the future. We have experimented empirically by placing the boundary further/closer from shore, but in all cases at distance greater than storm size R; in general, there are no significant changes in the coastal surges, providing the width of the continental shelf is greater than R.

along the boundary according to eq. (29) rather than cancel directly with static height gradient. For the unsheared system, it was not necessary to explicitly compute height gradients along the boundary.

D. Lateral Boundaries

We assume, during storm passage when surges are greatest, that the central area of the basin is not affected by lateral boundaries. This is borne out with empirical tests for various types of lateral boundary conditions, providing the lateral boundaries are sufficiently far from the basin center.

We set fictitious conditions on the boundary of $\partial V^*/\partial y^* = \partial V/\partial y = 0$; note that the boundary, and immediate neighboring region, has $\partial \eta/\partial y = 0$, figure 1. To compute for V^*, we dispense with the 2d momentum equation of eq. (12) and use the following uncentered positional operator

$$(31) \qquad {}^{B}D^{5}_{y^*} = \begin{vmatrix} -1. & & 0. & & -1. \\ & 4. & & 4. & \\ 0. & & -6. & & 0. \end{vmatrix} .$$

where B means bottom lateral boundary; a similar procedure is used for the top lateral boundary. With eq. (31) operating on V^*, and set to zero, then

$$(32) \qquad (V^*)^{k+1}_{n,1} = [4\{(V^*)^{k+1}_{n-1,2} + (V^*)^{k+1}_{n+1,2}\} - (V^*)^{k+1}_{n-2,3} - (V^*)^{k+1}_{n+2,3}]/6.$$

Note eq. (31) is no more than eq. (15) rotated 90° with no sign changes. For the top lateral boundary the rotation is 270° and eq. (31) reverses signs. We compute U^* and h with the first and third equations of eq. (12) but with spatial derivatives incorporating eq. (15) under proper rotation; also, eq. (16) and (30)* under proper rotation are used to compute U^*; the continuity equation in eq. (12) does not require eq. (16) since depths are not present.

E. Corner Points

There are four corner points, figure 1. A direct way to dispose of these points (and the lateral boundaries as well) would be to formulate a graduated absorptive condition so field values are zero on the lateral boundaries. However, until such time as this is investigated we compute on the corner

---

* Empirically, for long time runs, we have found that

$${}^{B}D^{5}_{x^*} = \tfrac{1}{2}\begin{vmatrix} 1. & & 0. & & -1. \\ & -4. & & 4. & \\ -2. & & 0. & & 2. \end{vmatrix}$$

gives better results.

points with an uncentered positional operator*, as

(33)
$$C_{D_{x*}} = \begin{vmatrix} & 1. & \\ -2. & & -1. \\ & 4. & \\ -3. & & 2. \end{vmatrix} \qquad C_{D_{y*}} = \begin{vmatrix} & -1. & \\ 2. & & -1. \\ & 4. & \\ -3. & & -2. \end{vmatrix} \quad 1.$$

where "C" means left-bottom-corner; similar forms exist for the other three corner points but rotated 90^{o}, 180^{o}, 270^{o}, and with proper sign changes.

On the coastal corner points, $\partial V^*/\partial y^* = 0$ gives V^* through eq. (33). The first momentum equation of eq. (12), with (16), and spatial derivatives incorporating eq. (33) under proper rotation, are used to compute "h"; in eq. (12), $U^* = 0$ and hence $\partial U^*/\partial t = 0$.

On the deep water corner points, $\partial V^*/\partial y^* = 0$ gives V^* through eq. (33). The first momentum equation of (12), with (16), and spatial derivatives incorporating eq. (33) under proper rotation, are used to compute U^*. The continuity equation is ignored since "h" is supplied by the storm itself.

5. AN EXAMPLE AND COMPARISON WITH AN UNSHEARED SYSTEM

The effects of a curving coastline are best demonstrated with a storm moving more or less alongshore. Such a storm track generates surges on a longer length of coastline compared to a landfall storm. The coast, at a distance from the basin center** can veer dramatically away from the baseline; consideration of this deviation from the baseline can be significant in surge generation.

---

* These forms are weighted combinations of two separate 5-point forms. Empirical tests with eq. (33) give better results than either of the two separate 5-point forms.

**By "basin center" we mean the mid-point of the baseline, figure 1.

As an example, consider hurricane Donna, 1960, which passed the Eastern Seaboard, figure 6. For meteorological input data (to generate driving forces) we specify:

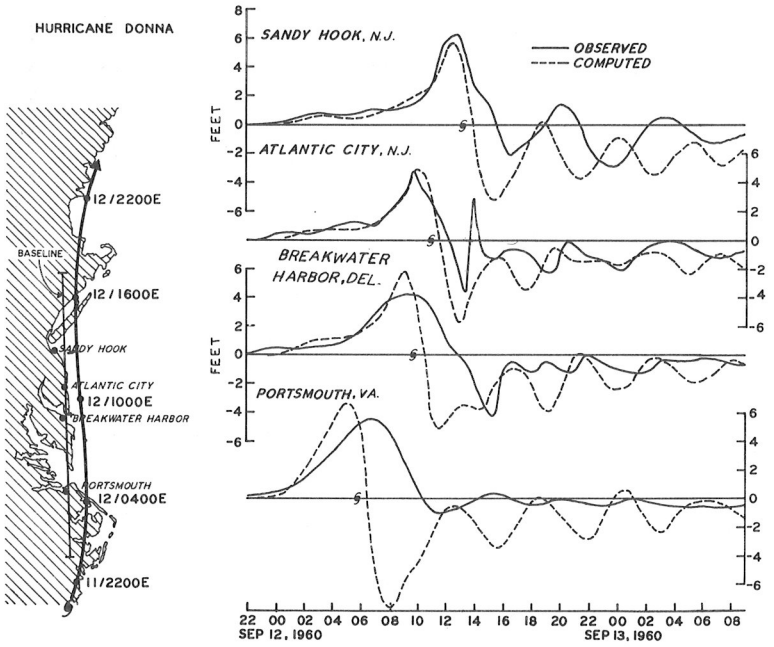

Figure 6.--Observed/computed time-history surges at four tide gages, generated by hurricane Donna, 1960. The computed surges are for the sheared system. Atlantic City is a coastal gage, whereas the other three gages are inside estuaries. "$\mathcal{S}$" means time-of-storm-abeam-of-tide-gage. The left side of the figure illustrates the storm track, and the "baseline" for the basin used in computations. The basin is centered at Cape May, N.J., just north of Breakwater Harbor.

1. initial and final pressure drops for a 24-hour span ($\Delta P_o, \Delta P_{24}$), where ΔP means difference between ambient and central pressure of the storm,

2. initial and final storm size (R_o, R_{24}), where "R" means distance from storm center to maximum winds, and

3. five storm positions at 6-hourly intervals.

For details on how these data are used to form 48 hours of driving forces, see Jelesnianski (1974) and Jelesnianski and Taylor (1973). From various sources, we have tentatively assembled initial and final pressure drops of 46 and 57 mb, a constant storm size of 40 statute mi., and five track positions as shown on figure 6.

The simulated coast of the basin is centered with a baseline at Cape May, just north of Breakwater Harbor; at the entrances to Chesapeake, Delaware, and Lower (Raritan) bays, there are fictitious vertical walls. Details of the simulated coast are not shown in figure 6 due to coarse scaling.

The sheared SPLASH II program was specially altered for Donna for 36 hr of model time to compute resurgences after storm passage (the operational program runs for 18 hr, 12 hr before storm passage at the basin center plus 6 hr thereafter).

We want to compare real data from Donna; these exist for four tide gages, figure 6. Three of the gages are located inside bays/estuaries (not the ocean side) and only Atlantic City lies on the open coast. The original gage data was modified by subtracting out predicted astronomical tide as well as sea level anomolies determined from monthly means (Harris 1963); the resulting data can be described as "meteorological" tide, for it is this tide we use for comparisons. We compare our model with surges generated from driving forces only; no attempt is made to compute with astronomical tide, nor interaction between astronomical and meteorological tide. The computed, time-history, surge profiles are for the sheared system.

In figure 6, the symbol "$\mathcal{S}$" locates "time-of-storm-abeam-of-gage". At any fixed times, the highest surge on the coast is associated with the storm; it moves along the coast with the storm as part of a forced wave; all following resurgences--behind the storm on the coast--are free waves. Such wave phenomena are discussed by Jelesnianski (1974). All four gages exhibit a general <u>rise</u> above sea level before storm arrival, followed by a general <u>fall</u> below mean sea level after storm passage. These phenomena*, before storm arrival, are sometimes called "forerunners"; note, these are computed by the model if the storm is initialized sufficiently back in time, and hence should not be construed as an initial set-up to be added onto the computed peak surge, Appendix C.

Figure 7a compares the computed envelopes of high waters on the simulated coast, generated by Donna, for the sheared and unsheared systems. In the unsheared SPLASH system, the natural coast (and forces) are shifted to the baseline, but the equations of motion (1) are not transformed to eq. (6).

Figure 7b compares observed time-history surges at Atlantic City and Sandy Hook against the sheared and unsheared systems. The sheared system is an improvement over the unsheared system.

---

* The opposite occurs if the storm moves in the opposite direction; i.e., a storm moving north along the west Florida coast, or a storm moving northwest along the northwest Florida coast. In such cases there is a general <u>fall</u> before storm arrival, followed by a general and rapid <u>rise</u> after storm passage. This situation is very deceptive to the surge forecaster if he is depending on the trend of tide gages to aid in forecasting.

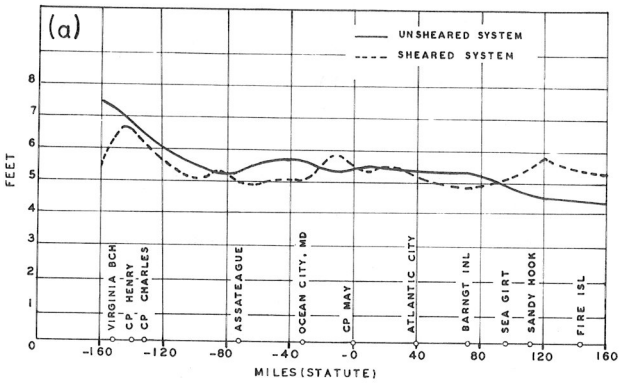

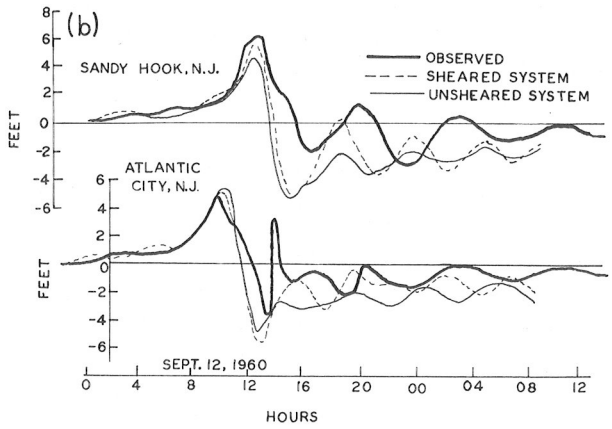

Figure 7a.--A comparison of computed surge envelopes generated by the sheared and unsheared models, for the Donna 1960 storm, see figure 6.

Figure 7b.--A comparison of observed time-history surges at Atlantic City and Sandy Hook, for hurricane Donna 1960, with the sheared and unsheared models.

The storm exited south of Portsmouth and made landfall north of Sandy Hook. The SPLASH models without the shear system compute acceptable surges about the basin's center; but for adjacent areas, where the coast deviates from the baseline, the computed surges may not be valid. With the sheared system, however, we can consider surges on adjacent areas if the coastal curvature is not dramatic and the coastline orientation does not deviate greatly (more than $\pm$ 45°) from the baseline; also, the baseline need not be tangent to the coast at the basin's center.

There is little difference in surge computations between the sheared and unsheared models at basin center, figure 7a; the small differences there are due to small coastal curvature and a baseline not quite tangent to the coast. the most significant differences are south of Cape Henry and north of Sandy Hook where the coast has greatest curvature and is orientated at a large angle with respect to the baseline. About Cape Henry the storm is exiting and the computed surge with the sheared system is smaller, but about Sandy Hook the storm is landfalling and the surge is larger; these discrepancies are due to a curving coast orientated at a large angle with the baseline. To compute surges in these two areas with the unsheared SPLASH models, we would need to compute in separate basins for short stretches of coasts that do not deviate significantly from a baseline; with the sheared system, however, the coast can deviate from a baseline and it is possible to compute along a greater stretch of coastline. The envelope of surges with the sheared system shows detail; in particular, where the coast is concave landward (a cape) the surges are smaller, and where the coast is concave seaward (a cove) the surges are larger.

In our model, the ocean is uncoupled from bays/estuaries; there are fictitious vertical walls at the mouths and we should not expect valid comparisons between computed surge values on the open coast and a tide gage inside the bay. The effects of a bay (feedback) on the mouth and surrounding open coast depends in part on storm size relative to size of the bay's major axis, the orientation of this axis to the ocean coast (perpendicular/parallel), and the orientation of the storm's track relative to the axis. Also, the mouth may act as a control so that the bay and ocean sides have different surge heights. On the Eastern Seaboard, the axis of bays are nearly perpendicular to the ocean coast and storm tracks are generally perpendicular to the axis. Under these conditions, the storm passes quickly across the bay mouths, the significant driving forces inside the bays have a short time span, and the ocean surges acting through the bay mouths have a lot to say about the response inside the bays. For different size bay axes, relative to storm size, the following may hold:

1. For short axis--such as Lower (Raritan) Bay--the time lag between events on the open coast (mouth) and inside the bay are small, with small local variations inside the bay, and the computed open coast surge is useful to represent conditions inside the bay.

2. For an intermediate-size axis--such as Delaware Bay--there are lags between events on the open coast and inside the bay. There are some local variations inside the bay, and reflections from the head to the mouth of the bay during the active time of the storm in the bay area may be present. These rejection surges complicate not only the surges at the mouth but also the surrounding coasts and our model as presently consituted cannot compute these additional events on the coast. The computed open coast surge does have some skill in representing conditions inside the bay in a coarse way.

3. For a large axis--such as Chesapeake Bay--there are large time lags between events on the open coast and deep inside the bay, some possibly significant local variations inside the bay, but during the active time of the storm in the bay area there are limited rejection surges affecting the mouth; i.e., the return period of the rejection surges are large, and storm tenure small, so that bottom stress and other phenomena have sufficient time to help dissipate the reflected surge. The computed peak surge of the forced wave has some skill in representing the peak surge inside the bay and not too far from the mouth, but following resurgences are not well represented inside the bay.

The Portsmouth gage is located about 20 mi. inside Chesapeake Bay, on a tributary, figure 6. The computed peak surge leads the observed by about 2 hr; this is to be expected, for it takes time for the open coast surge to reach into the bay. The amplitude of the computed peak surge is slightly larger than given by the gage; the amplitudes of the minimum surge and resurgences compare poorly with the gage values. Inasmuch as the gage is far removed from the mouth, and the mouth may act as a control, we don't know how pronounced the resurgences are at the ocean side of the mouth nor how well our computations fit there.

The Breakwater Harbor gage is located slightly inside Delaware Bay. The Bay is much smaller than Chesapeake Bay, and its major axis is larger (but not much larger) than storm size; in this situation, rejection surges (reflections from the head of the bay) may complicate the gage output. The amplitude of the computed peak surge is slightly larger than given by the gage; the amplitudes of the minimum surge and resurgences compare poorly to fairly with the gage values. Since the mouth may act as a control, we don't know how well the computed resurgences at the ocean side represent real ones.

The Atlantic City gage is located on the open coast where our model is applicable, and we expect useful results. The computed peak and minimum surge agree fairly well with observed. The short period "spike" at about 1400 hr is completely missed by the model; its duration is much smaller than the resurgences and possibly represents feedback and focusing from Delaware and other bays. The computed resurgences are well represented except for leading the observed values. Recall that the periods of the resurgences depend on storm speed, size, and distance from the coast (Jelesnianski 1974); hence,using a constant storm size of 40 statute mi. may be an oversimplification; the storm acquires extratropical characteristics--and possibly increasing size--as it moves into higher latitudes. We can easily change the period of the resurgences by allowing storm size to change with time--and this can be done well within meteorological accuracy--for a better representation of the resurgences.

The Sandy Hook gage is located inside Lower (Raritan) Bay, close to the entrance. The bay is much smaller than Chesapeake and Delaware Bays and even smaller than storm size; we therefore expect some useful results here. The computed resurgences lead the observed, just as at Atlantic City but even more so (due possibly to improper storm size), and the amplitudes are slightly off. The amplitude of the computed peak surge is slightly smaller. The sheared coordinate system recognizes coastal curvature and the large slant between Long Island and the mainland and this enables the model to compute larger surges than for an uncurved coast. Since the mouth may act as a control, we don't know how well the resurgences on the ocean side represent real ones.

6. SUMMARY AND CONCLUSIONS

The operational prediction of storm surges is almost exclusively concerned with the rise of coastal waters generated by storms. The circulation patterns on the shelf and in deep ocean waters, are of casual interest, if at all. In fact, they are a means to an end; that is, an aid to calculate coastal surge heights.

Model basins, with vertical walls representing the coast, need not be broken in stairstep fashion for convenience in numerical computations. Stairstep boundaries distort the natural coast precisely where computational results are required. In our methods, the simulated coast curves naturally and continuously, and we distort instead the remaining boundaries where computational results relative to the coast need not be accurate.

Our model computes surge heights on the coast, as well as parallel flow. Some numerical schemes, in contrast, perform no computations whatever on the coast. Such schemes compute surge heights one grid space from the simulated (stairstep) coast; they are useful to compute circulation patterns on basin interiors but not necessarily surges on coast lines.

The sheared coordinate model

1. shifts (transforms) curved coasts onto a straight "baseline" which touches the coast midway on the basin, figure 1,

2. transforms a plane surface with curved boundaries, truncated from the ocean shelf, into a rectangle, and

3. transforms the equations of motion to accommodate the sheared coordinate system.

Finite-difference forms are used on the transformed rectangle, and the transformed coast now falls on a grid line and not between grid lines; i.e., stairstep boundaries are not required. Our model does not route water overland.

Coastal curvature affects coastal surge generation, and this is recognized by the sheared system. Should land jut out into the sea (a cape) all other things the same, the surges on the curved coast are smaller; whereas, if sea juts out into the land (a cove), then the surges are larger. These actions are more pronounced the shallower the basin.

The natural coast, at large distances from the basin center, will slant significantly from a baseline. Compared to the unsheared SPLASH models, the sheared model is more useful with non-landfall storms or for storm tracks with a small angle of attack to the coast. In such cases the sheared system accounts for a large segment of curved coast exposed to surge generation; whereas, a linear geographical coastline in the unsheared models is an oversimplification to simulate the naturally curved coastal segment.

The sheared model, on the other hand, is not necessarily an improvement if the storm track is nearly perpendicular to the coast and strikes the coast near basin center. In such cases only a small segment of coast is exposed to surge generation and this segment can be approximated with a linear line as used in the unsheared models. At short distances from the basin center the natural coast does not slant significantly from the baseline, even if there is some coastal curvature there. Of course, if there is significant curvature of the coast at landfall point, then the sheared system is an improvement.

In the vicinity of basin center there is little improvement with the sheared model, no matter what the storm track. This is so because the coast does not slant significantly from the baseline; an exception of course would be strong coastal curvature at basin center. The greatest improvement occurs when surges abound on a large coastal segment and portions of the coast slant significantly from a baseline. This means that one computational effort is usually

sufficient when storms affect a lengthy coastline (less than 300 mi.) with surges. In contrast, the unsheared models require several runs to handle such a coast; the separate runs compute with succeeding basins and baselines that effectively simulate only a small portion of the coast in the vicinity of succeeding basin centers.

A disadvantage of our model is shorter time steps in numerical computations. The time step varies inversely as the slant of the coast relative to the baseline; a coarse stability analysis shows this to be true. For this reason, we do not permit any part of the coast in our model to slant by more than $\pm 45^{o}$ with respect to the baseline.

ACKNOWLEDGMENTS

I am deeply indebted to Albion Taylor for his many helpful suggestions and the many friendly hours of discussion on storm surge hydraulics.

Work on this project was partially supported by the Federal Insurance Administration (FIA) of the U. S. Department of Housing and Urban Development (HUD), under Interagency Agreement No. IAA-H-10-76, dated November 24, 1975, Project Order No. 1.

REFERENCES

Barrientos, Celso S., and Jelesnianski, Chester P., 1973: Storm surge shoaling corrections along the Gulf Coast, A Study for Federal Insurance Administration, U. S. Dept. of Housing and Urban Development, Dec., 41 pp.

Birchfield, G. E. and Murty, T. S., 1974: A numerical model for wind-driven circulation in Lakes Michigan and Huron. Mon. Wea. Rev., 102, Feb., 157-165.

Harris, D. Lee, 1963: Characteristics of the hurricane storm surge, Technical Paper No. 48, Weather Bureau, U. S. Department of Commerce, Washington, D. C., 139 pp.

Jelesnianski, Chester P., 1967: Numerical computations of storm surges with bottom stress, Mon. Wea. Rev., 95, Nov., 740-756.

_____, 1970: Bottom stress time-history in linearized equations of motion for storm surges. Mon. Wea. Rev., 98, June, 462-478.

_____, 1972: SPLASH (Special Program to List Amplitudes of Surges from Hurricanes): I. Landfall Storms. NOAA Technical Memorandum NWS TDL-46, Techniques Development Laboratory, National Weather Service, NOAA, U. S. Dept. of Commerce, Washington, D.C., April, 52 pp.

_____, and Taylor, Albion D., 1973: A preliminary view of storm surges before and after storm modifications, NOAA Technical Memorandum ERL WMPO-3, Weather Modification Program Office, ERL, NOAA, U. S. Dept. of Commerce, Washington, D.C., May, 33 pp.

_____, 1974: SPLASH (Special Program to List Amplitudes of Surges from Hurricanes): II. General Track and Variant Storm Conditions. NOAA Technical Memorandum, NWS TDL-52, Techniques Development Laboratory, National Weather Service, NOAA, U.S. Dept. of Commerce, Washington, D.C., Mar., 55 pp.

Platzman, George W., 1963: The dynamical prediction of wind tides on Lake Erie, Meteorological Monographs, 4, Sept., 44 pp.

Wanstrath, J., Whitaker, R. W., Reid, R. O., and Vastano, A., 1976: Storm surge simulation in transformed coordinates, Texas A and M, to be published.

APPENDIX A: STABILITY CRITERIA

This Appendix discusses a gross stability criteria for an abbreviated form of the sheared equations of motion of the main text, given as

$$\begin{aligned} \partial U^*/\partial t &= -gD(a_2\,\partial h/\partial x^* - a_1\,\partial h/\partial y^*) + f(a_2 V^* + a_1 U^*) \\ \partial V^*/\partial t &= -gD(-a_1\,\partial h/\partial x^* + \partial h/\partial y^*) - f(a_1 V^* + U^*) \\ \partial h/\partial t &= -\partial U^*/\partial x^* - \partial V^*/\partial y^* \end{aligned} \tag{A1}$$

where $a_1 = d\eta/dy = \eta_y$; $a_2 = 1 + \eta_y^2$.

A coordinate transformation, $x^* = x - \eta(y)$, $y^* = y$, shifts the shoreline boundary onto $x^* = 0$, see eq. (6) of the main report. For a study of stability, the surface and bottom stresses, and pressure gradient driving force are not considered. For convenience the depth or bathymetry is taken as constant; that is, the maximum depth of a basin.

The time and space derivatives are approximated by eq. (9-11b) in the main text. Setting these equations into eq. (A1) gives

$$\begin{aligned} (U^*)^{k+1}_{m,n} &= (U^*)^{k-1}_{m,n} - \alpha[a_2 D^5_{x^*} - a_1 D^5_{y^*}]h^k_{m,n} + \gamma[a_2 (V^*)^k_{m,n} + a_1 (U^*)^k_{m,n}] \\ (V^*)^{k+1}_{m,n} &= (V^*)^{k-1}_{m,n} - \alpha[-a_1 D^5_{x^*} + D^5_{y^*}]\, h^k_{m,n} - \gamma[a_1 (V^*)^k_{m,n} + (U^*)^k_{m,n}] \\ h^{k+1}_{m,n} &= h^{k-1}_{m,n} - \beta[D^5_{x^*}(U^*)^k_{m,n} + D^5_{y^*}(V^*)^k_{m,n}] \end{aligned} \tag{A2}$$

where $\alpha = gD\,\Delta t/(2\Delta s)$, $\beta = \Delta t/(2\Delta s)$, $\gamma = f2\Delta t$.

Consider now formal solutions for the transport and height field consisting of individual terms

$$(U^*, V^*, h)^{k\Delta t} = (U^*, V^*, h)^0 \lambda^k \tag{A3}$$

where $(U^*, V^*, h)^0_\alpha e^{i(am,bn)\Delta s}$, and $a = 2\pi/L$, $b = 2\pi/W$ are spatial wave numbers.

The formal solution permits

$$\begin{aligned} (U^*, V^*, h)^{(k+1)\Delta t} &= \lambda^2 (U^*, V^*, h)^{(k-1)\Delta t} \\ (U^*, V^*, h)^{k\Delta t} &= \lambda (U^*, V^*, h)^{(k-1)\Delta t} \end{aligned} \tag{A4}$$

Setting eq. (A4) into eq. (A2) gives, after some rearrangement

$$(A5)\quad \begin{vmatrix} \lambda^2 - 1 - \lambda\gamma a_1 & -\lambda\gamma a_2 & i\alpha\lambda(a_2\nu' - a_1\nu'') \\ \lambda\gamma & \lambda^2 - 1 + \lambda\gamma a_1 & i\alpha\lambda(-a_1\nu' + \nu'') \\ i\lambda\beta\nu' & i\lambda\beta\nu'' & \lambda^2 - 1 \end{vmatrix} \begin{vmatrix} (U^*)^{k-1}_{m,n} \\ (V^*)^{k-1}_{m,n} \\ h^{k-1}_{m,n} \end{vmatrix} = 0$$

where $\nu' = 4 \sin a\Delta s \cos b\Delta s$, $\nu'' = 4 \sin b\Delta s \cos a\Delta s$.

In order for eq. (A5) to hold, then

$$(A6)\quad (\lambda^2 - 1)\,[(\lambda^2 - 1)^2 + \lambda^2\gamma^2 + \lambda^2\alpha\beta(\nu''^2 - 2a_1\nu'\nu'' + a_2\nu'^2)\,] = 0$$

or

$$(A7)\quad \lambda^4 - 2\lambda^2\left[1 - \frac{\gamma^2 + \alpha\beta(\nu''^2 - 2a_1\nu'\nu'' + a_2\nu'^2)}{2}\right] + 1 = 0$$

for stability it is required that $|\lambda^2| \leq 1$; then from eq. (A7)

$$(A8)\quad \frac{\gamma^2 + \alpha\beta(\nu''^2 - 2a_1\nu'\nu'' + a_2\nu'^2)}{4} \leq 1$$

or with $\alpha\beta$ replaced by $gD(\Delta t^2) / (4\Delta s^2)$, $\gamma = f2\Delta t$,

$$(A9)\quad \Delta t^2 \leq \frac{\Delta s^2}{f^2\Delta s^2 + \frac{gD}{16}(\nu''^2 - 2a_1\nu'\nu'' + a_2\nu'^2)}$$

The term

$$\Delta = \nu''^2 - 2a_1\nu'\nu'' + a_2\nu'^2$$

in eq. (A9) is a positive definite form. It can be written as

$$\Delta = 4\,[(2 - 2\eta_y + \eta_y^2)\sin^2(a+b)\,\Delta s + (2+2\eta_y+\eta_y^2)\sin^2(a-b)\,\Delta s + 2\eta_y^2 \sin(a+b)\,\Delta s \sin(a-b)\,\Delta s\,].$$

But reaches its maximum when $a = (\pm \pi/2)/\Delta s$ and $b = 0$. In this case

$$\Delta = 16\,(1 + \eta_y^2).$$

Hence,

$$(A10)\quad \Delta t \leq \frac{\Delta s}{\sqrt{f^2\,\Delta s^2 + gD\,(1 + \eta_y^2)}}$$

where the depth "D" is maximum depth of a basin. Δt corresponds to the extreme upper limit of stability, or alternately to the extreme lower limit of instability, for very short waves in deep water. Factors not included in the above analysis, such as the effects of boundary conditions or curvature of the coast (η_{yy} not identically zero), may then induce productions and amplification of such short waves. To avoid such effects, a safety margin is used; in practice, one should not set Δt equal to the right side of eq. (A10). Applying a safety factor of $(2)^{-\frac{1}{2}}$ to the right side of eq. (A10) usually suffices. Since $f\Delta s$ is usually much less than $\frac{1}{2}$, we may drop the coriolis term and establish a practical stability criterion

$$\Delta t \leq \Delta s / \sqrt{2\, gD\, (1 + \eta_y^2)} \ .$$

If η_y is to be limited to $|\eta_y| \leq 1$, we may set

(A11) $$\Delta t = \Delta s / 2\sqrt{gD} \ .$$

APPENDIX B: SHEARED COORDINATES

This Appendix describes several coordinate systems, not necessarily orthogonal, to describe a meandering coastline, figure B1. For illustrative purposes, the four systems have been localized, with origin placed at a coastal point of interest, and with a flow vector $\vec{V}$ issuing from the origin. In all four systems the parallelogram law (addition of vectors) holds.

In figure B1.a, a coastline at point "O" has a local slant ($\pi/2-\theta$) from a fixed axis or baseline (call it relative NORTH). The vector $\vec{V} = Ui + Vj$, where (i,j) are unit vectors, have components (U,V) on the NORTH and EAST, or (x,y), orthogonal axes. The components are cumbersome to apply on a meandering coast; e.g., if the vector $\vec{V}$ is parallel to the coast, then the boundary condition of no normal component at the coast is $U \sin\theta - V \cos\theta = 0$.

Suppose now the NORTH and EAST axis are rotated ($\pi/2-\theta$) to form a natural coordinate system so that $\vec{V} = U_n i_n + V_t j_t$, figure B1.b. Then the boundary condition $U_n = 0$ is less cumbersome to apply at the coast. However, the axes are not fixed and meander with the coast. To use this system it is necessary to develop a general-curvilinear, conformal transformation to maintain orthogonality of axes on a meandering coast. Such a transformation has been explored by Wanstrat et. al., (1975).

We want to directly recognize a meandering coast on a grid scheme, without recourse to a general-conformal transformation of curvilinear coordinates. To do so, a particularly simple system can be formed if the constraint of orthogonal axes in the original plane is dispensed with. Even though non-orthogonal forms are not popular and rarely used in ordinary applications, they do have powerful properties and useful advantages for particular cases. In this Appendix we give a brief summary on non-orthogonal frames for those readers unfamiliar with it. However, instead of a general and concise mathematical overview in "n" space with tensor notation, we restrict ourselves to a plane (2 space) for useful application in storm surge prediction.

We must start with two reference directions, and for convenience we choose the following:

1. a direction perpendicular to the straight baseline (call it the x*-axis, and noting the that the x-axis and x*-axis are identical),

2. a direction parallel to the meandering coast (call it the y*-axis).

One can look on the axes as a pair of scissors, one blade (the coast) having the freedom to open or close. It is possible to span this space in two strongly different ways, each with two base vectors as follows:

1. (i_*, j_*) base vectors parallel to the two axes, figure B1.c,

2. (i*,j*) base vectors perpendicular to the two axes, figure B1.d.

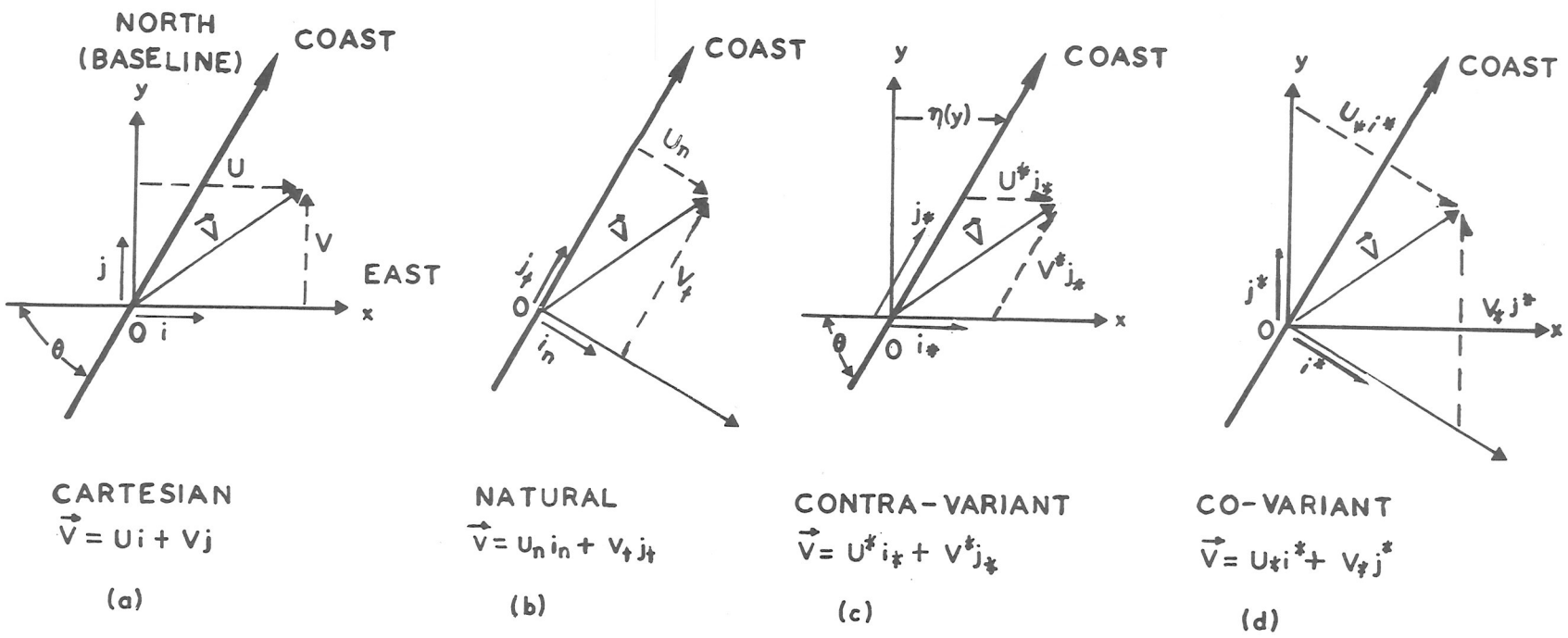

Figure B1.--Four different coordinate systems, base vectors, vector components, and component numbers for a meandering coast. The contra-variant system is used in this report.

Each of the (i_*,j_*) base vectors is drawn with a half arrow, the barb to the left; each of the (i^*,j^*) base vectors is drawn with a half arrow, the barb to the right. When both axes are perpendicular (orthogonal) in a cartesian frame, the separate base vectors (i_* and i^*, j_* and j^*) coalesce into an arrow and there is no difference between the two systems. We call the (i_*,j_*) system contra-variant, the (i^*,j^*) system co-variant. Unless the axes are orthogonal, the components of one system are completely different from components in the other.

Any vector $\vec{V}$ can be broken into two component numbers, directed along base vectors. The components are vectors, with magnitude proportional to the magnitude of the base vector; it is important to realize that the base vectors need not be of unit magnitude. Usually in a cartesian, orthogonal frame, the absolute value of a vector component is simply called the "component", it being understood the component vector is a component number multiplied by a unit base vector. For a non-orthogonal frame in a plane, or for a curvilinear orthogonal coordinate system in the plane, a component vector is a component number multiplied by a base vector that may or may not be of unit magnitude. In this case, a component number is the absolute value of a component vector divided by the absolute value of a basis vector.

In the contra-variant form, the component vectors are written $(U^*i_*V^*j_*)$, and the co-variant from (U_*i^*,V_*j^*). The component numbers are not the same in each frame, unless the axes are orthogonal. In the orthogonal frames of figures B1.a, B1.b, the dot products for unit base vectors are

(B1) $\quad i\cdot j = i_n\cdot j_t = 0; \qquad i\cdot i = j\cdot j = i_n\cdot i_n = j_n\cdot j_n = 1.$

In the non-orthogonal frames,

(B2) $\quad i_*\cdot j^* = i^*\cdot j_* = 0,$

and we wish to form, in conformity with the second set of equations in (B1),

(B3) $\quad i_*\cdot i^* = j_*\cdot j^* = 1.$

This is possible if we set,

(B4) $\quad |i^*| = |j_*| = 1/\sin\theta$

Then,

$$
\begin{aligned}
U^* &= \vec{V}\cdot i^* = [U^* i_* + V^* j_*]\cdot i^* = U_n \sin\theta \\
V_* &= \vec{V}\cdot j_* = [U_* i^* + V_* j^*]\cdot j_* = V_t \sin\theta .
\end{aligned} \tag{B5}
$$

The component numbers (U^*, V_*) are no more than the natural "components" (U_n, V_t), scaled by $\sin\theta$. Eq. (B5) is an important conclusion for a coastal boundary condition. If there is no transport through the boundary, then $U_n = U^* = 0$ is a boundary condition. Because of this important property, contra-variant, component numbers are used in the prediction equations for storm surges in this report. Conceivably, one could postulate no parallel flow along a boundary; in this case $V_t = V_* = 0$ would be a boundary condition and co-variant, component numbers would be used.

To use the contra-variant, component numbers in our prediction equations, we make use of a transformation.

$$
\begin{aligned}
x &= x^* + \eta(y), \quad \eta(y) \text{ is the distance of the coast from the baseline, directed along the } x^*\text{-axis} \\
y &= y^*
\end{aligned} \tag{B6}
$$

or,

$$
\begin{aligned}
dx &= dx^* + \eta_y dy^*, \quad \eta_y = d\,\eta(y)/dy = \cot\theta \\
dy &= dy^*
\end{aligned} \tag{B7}
$$

or,

$$
\begin{aligned}
U &= U^* + \eta_y V^* \\
V &= V^* .
\end{aligned} \tag{B8}
$$

The transformation eq. (B6) preserves areas. To prove this, the Jacobian of the transformation must be 1,

$$
J = \begin{vmatrix} \frac{\partial x}{\partial x^*} & \frac{\partial x}{\partial y^*} \\ \frac{\partial y}{\partial x^*} & \frac{\partial y}{\partial y^*} \end{vmatrix} = \begin{vmatrix} 1 & \eta_y \\ 0 & 1 \end{vmatrix} = 1. \tag{B9}
$$

We visualize a shifting of the axes in figure B1.c, by means of the shift function $\eta(y)$, through eq. (B6), onto an image plane; the axes in the image plane are orthogonal; see figure 2 of the main text.

The gradients have the following forms,

$$
\frac{\partial}{\partial x} = \frac{\partial x^*}{\partial x}\,\frac{\partial}{\partial x^*} + \frac{\partial y^*}{\partial x}\,\frac{\partial}{\partial y^*} = \frac{\partial}{\partial x^*} \tag{B10}
$$

$$\frac{\partial}{\partial y} = \frac{\partial x^*}{\partial y}\ \frac{\partial}{\partial x^*} + \frac{\partial y^*}{\partial y}\ \frac{\partial}{\partial y^*} = \frac{\partial}{\partial y^*} - \eta_y \frac{\partial}{\partial y^*} \ .$$

Hence, when eq. (B8) and (B10) are plugged into the original equations of motion, we then transform the original equations of motion into contra-variant, component numbers. This has been done in the main text.

To set the natural system in terms of the contra-variant, component numbers,

$$dx_n = dx \sin\theta - dy \cos\theta = \frac{dx - \eta_y dy}{\sqrt{1 + \eta_y^2}} \quad , \sin\theta = \frac{1}{\sqrt{1 + \eta_y^2}}$$

(B11)

$$dy_t = dx \cos\theta + dy \sin\theta = \frac{\eta_y\ dx + dy}{\sqrt{1 + \eta_y^2}} \quad , \cos\theta = \frac{\eta y}{\sqrt{1 + \eta_y^2}}$$

where (x_n, y_t) are on the natural system of figure B1.b. Combining eq. (B7) and (B11) gives

(B12)
$$dx_n = dx^* / \sqrt{1 + \eta_y^2}$$
$$dy_t = [\eta_y dx^* + (1 + \eta_y^2)\ dy^*] \ / \sqrt{1 + \eta_y^2}$$

or for flow

$$U_n = U^* / \sqrt{1 + \eta_y^2}$$

(B13)
$$V_t = [\eta_y U^* + (1 + \eta_y^2)\ V^*] \ / \sqrt{1 + \eta_y^2} \ .$$

If the flow vector $\vec{V}$ is parallel to the coast, then the boundary condition $U_n = 0$ implies $U^* = 0$ from eq. (B13).

APPENDIX C: SOME SPECIAL PROBLEMS WITH SURGE MODELS

There are many troublesome procedures to deal with before a researched surge model can be developed for operational planning and prediction. Application of these procedures has a lot to say about the computed surge output. A model will stand or fall depending on how it is applied, no matter the sophistication of the mathematics or physics of the model.

In this Appendix, the author gives some personal views on some special aspects and problems with model calibration, input boundary conditions for bays and estuaries, initialization of models, storm models and driving forces, short gravity-wind waves, and wave set-up.

A. Comments on Model Calibration and Input Boundary Conditions

A set of partial differential equations, plus <u>properly</u> posed boundary conditions on simulated basins, is called a system. A surge model considers the activity or action in a system and can be summarized as

system

input $\rightarrow$ or $\rightarrow$ output

black box

The system (black box) contains several dangling coefficients which need to be pre-set or determined experimentally. The coefficients can be viewed as tuning knobs on the black box; they connect surface and bottom stress, admittance at bay mouths, weir contractions, etc., to the equations of motion of the system.

The input can be storm driving forces, input boundary values (surge or astronomical tide at selected boundaries), etc. The output is the final product of the model; it can be coastal surges, transport, etc. The model runs from left to right, output from input. The inverse, input from output, is rarely attempted because use of the model for this situtation may be over-specified and improperly posed.

For any surge model with a given input, a pre-set position of the knobs on the black box has a great deal to say about the output. The knobs (coefficient values) are a result of physical approximations and are a measure of the ignorance of subtle dynamic phenomena in the equations of motion.

To test a model, historical input data are sent through the box and the knobs are then adjusted until the output agrees in some sense with historical measurements; this is called calibration and represents the major development effort for future production runs. Calibration is sometimes performed with data from a single storm and the coefficients set as fixed constants. It does not automatically follow that such a calibration can be universally applied. The knobs have many degrees of freedom, and data from a single storm may not be sufficient for calibration with constant coefficients;

this is equivalent to solving many unknowns with too few equations. Also, data from a single storm can be of poor quality, too sparse, etc., to effect a sound calibration. However, if the meteorology is reliable, and if the coefficients are physically related from experimental evidence, then the calibration is useful.

In a utilitarian sense, massive amounts of data, for a range of storm situations, are desirable to set the knobs for a general calibration. This of course is not always possible and one must do with the data on hand. However, before accepting a model for production runs, one must ascertain the worth and range of the calibration according to type basin and storm condition.

Shelf models have fewer knobs to deal with on the black box than bay models; also, the dynamics and boundary conditions are simpler. The knobs can be easily tuned with massive amounts of data from many types of basins, with many historical storms having a large range of conditions. The coefficients can be universally set as best fit constants for a global or large area and for all observed storm conditions; the surge output is not limited to a local region (a single basin) for a small range of storm conditions. The output, of course, does not fit the observed data perfectly, but does so in some best fit sense. It is an article of faith that the model can then be interpolated into regions where no data from historical storms are available.

In the SPLASH model which uses linearized equations of motion and a given storm model, the coefficients to be calibrated are eddy viscosity, bottom slip, and surface drag. The surge at the coast is weakly sensitive to the eddy and slip coefficients, but directly proportional to the drag coefficient. (If non-linear equations are used, the surge is much more sensitive to the eddy and slip coefficients.) After pre-setting the eddy and slip coefficients from experimental and empirical testing, the drag coefficient was then fitted as a fixed constant to accomodate surge data observed in many basins with many historical storms. Such a calibration does not give ideal results for a particular storm situation; its usefullness depends on how well the computed results of the model agree for a range of storms and basins, Jelesnianski (1972), page 28.

For bay models the situation is not so direct because of complicated dynamics and lack of data. It is doubtful if all the coefficients can be universally set as fixed constants, for all bays, and for all storm conditions. They may be set as local constants in separate bays for a limited range of storm conditions. A calibration requires coefficients of the system to represent dynamic ignorance in the equations of motion; this means simple models dealing with intricate bay physics have coefficients that may not be constant. A further difficulty is the severe limitation of data for calibration purposes in separate bays. In this situation, most of the coefficients are preset and only one or two are calibrated as local constants to fit the model's output to the limited data.

There can be objections to this abbreviated technique if the calibration is insufficiently general for a range of storm conditions, or if the calibration is done haphazardly. With the same data set, there are many ways to preset a portion of the system coefficients and each way may give a different

calibration for the remaining coefficients. When limited data are used, a misuse of the art of calibration can hide many sins of omission and commission. In fact, it is almost always possible to calibrate any model to effect a good verification with observed data from a single event; this by itself does not describe the character of the model, its strengths and its weaknesses.

A bay model calibrated directly with limited data and most coefficients pre-set as constants may be an oversimplification. Some models are calibrated for astronomical tide only; the coefficients for surface drag, overtopping of barrier islands, etc., are pre-set. Others use no calibration whatever and all the coefficients are pre-set. Such models are generally developed with a "make-it-work" attitude, concentrating solely on one particular area, and the user must be aware of the limitations; of course, they give meaningful insight for the mechanics of bay surges, but the output should be viewed with some discretion for planning or forecasting purposes. If a production run uses a radically different storm than used for calibration, then the output must be viewed with extreme caution.

Shelf models are sometimes used to generate boundary conditions for bay (estuary) models; usually, the models are uncoupled and feedback to the shelf model is ignored. At times this system works very well, but dynamically it can be a dangerous procedure.

To justify uncoupling of the models, it is assumed that events inside the bay have little effect on events outside the bay. In many cases, the input boundary data have greater influence in generating surges inside bays than driving forces do; hence, we can at times be cavalier with driving forces inside bays but not on the ocean shelf.

There are troublesome problems with broken coast entrances. For example, a bay mouth is usually constricted, possibly with a sill, and this gives complicated dynamics. The mouth can act at times as a control (height-discharge relation) to sustain large height differences over the bay and ocean sides. In this situation there can be large energy losses across the control, and simple linear equations of motion as well as energy conserving flow are then suspect. It is especially dangerous in these situations to use ocean-side surges from uncoupled shelf models as boundary data for bay sides.

After storm passage, figure 6, there are large height differences between observed-bay-side and computed-ocean-side surges. This does not mean that the computed-ocean-side surges are totally wrong; there is such a rapid change in flow* with passage of an alongshore moving storm that a mouth may be forced to act as a control and it is then dynamically possible to maintain large height differences. It is a mistake, however, to directly use the computed-ocean-side surges as boundary values on the bay side [similarly, to use the observed-bay-side surges as input boundary data for the shelf model, see eq. (27)].

---

* For landfalling storms, the flow change with storm passage is not as rapid.

One can use control features such as "downdrafts/updrafts" for sub-critical flow, or occurrence of critical flow at the mouth followed by a quasi-stationary hydraulic jump at a short distance from the mouth; also, if a coupling of the heights at bay and ocean sides is made to fit the dynamics, such as conservation of momentum, then this approach may be viable. It may be useful to use the computed-ocean-side surges (from an uncoupled shelf model) with the occurring action of a control at the mouth; the control then acts at times as a brake by backing-up water in the bay, and the computed-ocean-side surge may be representative in a coarse way.

If controls are used in a coupled bay/shelf model with one successful verification, it does not necessarily follow that the calibration will be suitable for all storm situations. By their nature controls can be sensitive to the existing flow and calibration coefficients; controls such as weirs, nozzles, overtopping of barriers, etc., can vary with the surge situation. If the model coefficients change with the flow situation, then the calibration is more reliable.

The practice of immediate applications for operational or planning purposes after one simulation result is premature. Instead, many tests should first be performed with a horde of simulated storm situations to protect against future surprises. The model's grid size should be optimized to the point where no siginficant changes occur with smaller grid sizes, and this should hold for all anticipated storm situations. Sensitivities at mouths, inlets, overtopping etc., should be ascertained before a model is considered operational. Should model results be sensitive to small changes in shelf/bay geometry, barrier heights, mouth depths, etc., or to meteorological parameters, then the model is suspect; in this situation subjectivity easily becomes rampant and physics just as easily ignored.

When judging surge models, the following may apply:

1. Do not judge the efficacy of a model merely by a comparison of observed and computed surges from a single storm event. Such a comparison is not necessarily relevant. Surge and storm models, no matter how primitive, can almost always be calibrated with pre-set coefficients to reflect a single storm event. However, if the coefficients recognize a changing flow situation (based on experimental evidence), then the calibration can be effective.

2. The efficacy of a surge model can be judged when comparing observed and computed surges for two or more vastly different storms affecting the same geographical area. It does not follow that the same calibration can be extended to a vastly different geographical area.

3. Do judge the efficacy of a model that has been universally calibrated with a multitude of basins and historical storm events. The comparison of computed and observed surges should fall within some statistical level of acceptability. Do not reject the model out of hand if it generates poor quality surges for a particular or rare storm event; the fault can lie with poorly measured

meteorological parameters, a rare or unusual storm whose character is not properly portrayed with the storm model, the generation of special and rare dynamic effects that the model is not geared to handle, etc.

4. Do not expect any model to be perfect.

B. Some Comments on Initialization of Models

Ideally, the storm surge is defined as the water height of a long gravity wave generated by a storm, in the absence of astronomical tide and other phenomena such as "wave set-up" from breaking wind waves. For practical forecasting, the predicted astronomical tide is superimposed onto the computed surge after computations are completed and without regard to any non-linear interaction with the surge; wave set-up may be added or incorporated in the computations. It is possible to compute with astronomical tide, but there is always a phasing problem with the storm surge because the predicted space/time track of the storm is usually significantly in error.

There are many ways to initialize surge models. One principal to remember is, initialization procedures become more important the closer the storm is initially positioned to shore. If the initial position of the storm is close to shore, then the coastal surge may already be significant and must be accounted for.

Sometimes, models are initialized with a statistical average of observed surge heights, or else historical surge heights for each event, so-many-hours before landfall; sometimes to finalize calibration, an ad-hoc initial set-up is used to force agreement between computed surges and observed data; sometimes models are initialized with a quiescent sea for a specified datum, and after computations an initial set-up is added onto the computed surge; sometimes the initial set-up is ignored completely.

Concepts on initial set-up vary and there are disagreements. Initial water heights (other than astronomical tide) can be broken into at least two categories, storm and non-storm induced. By non-storm induced is meant coastal sea level anomalies in the absence of storm effects; that is, seasonal or long term residuals of the astronomical tide not a concomitant of storms. For forecasting purposes the anomaly is determined several days before storm arrival by comparing differences between observed and predicted tide levels.

A local or anomalous change in sea level induced by vagaries in say, semi-permanent meteorological systems on the sea, sea temperatures, general oceanic flow, upwelling, etc., is the writer's concept for non-storm induced set-up. The resulting local change in sea level (at a coastal point or length) is then one type of "initial set-up" if it occurs before-during-after storm passage; the "after" portion is not really germane, but then one is not certain if the anomaly exists for the important "during" portion.

Harris (1963) suggests several ways to measure sea level anomalies for historical storms; for example, the difference between average mean sea level for a month and an observed monthly mean of coastal water heights, and the storm affecting the coast midway in the month. The effect of the surge on the monthly mean usually is small.

By storm induced is meant coastal sea level rises generated by a storm as a precursor or forerunner; they can be looked on as quasi-steady state when the storm is distant from shore but yet affecting coastal areas; usually, one day or less before landfall. Forerunners do not occur with all storms; in fact, with many storms there are sea level falls before storm arrival. Positive forerunners could be surge, wave set-up, or a combination of both. Wave set-up is discussed in a later section.

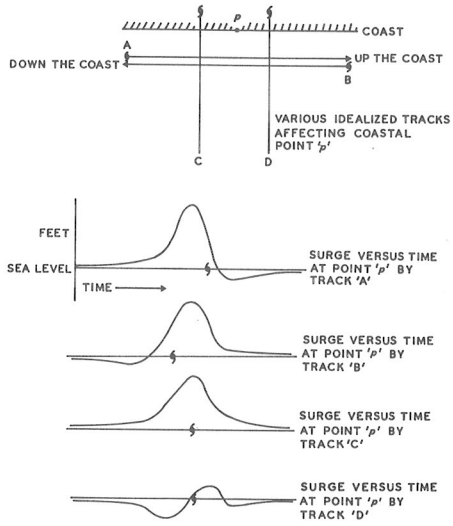

Figure C1.--Idealized time-history, surge profiles at point "p" on the coast for four selected storm tracks. Astronomical tide and sea level anomolies are not included.

Figure C1 shows several ways that initial set-up can occur during storm activity. The idealized time-history surge profiles at a coastal point are portrayed without astronomical tide, sea level anomaly, or wave set-up; if there were an anomaly the entire profiles would merely move up or down the ordinates, whereas the tide can be superposed (assuming no non-linear interactions), and wave set-up requires specialized treatment. A time-history, surge profile has tail ends that feather in to sea level; they are a form of set-up. These tail ends, before and after storm arrival, change slowly with time and are in a quasi-steady state until the fury of the storm affects the coast; they are dynamically induced by the storm and should not be added onto the computed surge. The formation of quasi-steady state sea level on the coast, before and after storm passage, varies as storm track relative to the coast. The slower the storm speed, the longer the duration of the tail ends on the time-history surge profile.

In an idealized sense, for simplicity of presentation, consider two types of storm track, out of phase by 90^{o} or 270^{o}; these are perpendicular and parallel to the coast. Both tracks have sub-forms that affect coastal surges dif-

ferently at a coastal point, and in particular affect the tail ends of the surge profiles.

For alongshore moving storms, the SPLASH model, and observations, agree as follows:

1. For storms moving up the coast

    a. high waters precede the storm
    b. low waters follow the storm

2. For storms moving down the coast

    a. low waters precede the storm
    b. high waters follow the storm

The storm track need not be precisely parallel to the coast; it need only have a component of track along the coast. Naturally, there are variations from the ideal cases, including wave trains (Jelesnianski 1974); see figure 6 of this report for a fast moving storm. Some situations that can cause variations are:

A. A storm that changes its character along a track (size, pressure drop, speed, etc.) so that a. or b. above, in 1. and 2., is more dominant.

B. The track curves dramatically so that only one of a. and b. occurs.

C. The coast curves sharply so that only one of a. and b. occurs.

For landfall storms perpendicular to the coast, the SPLASH models, and observations, agree as follows:

1. For storms landfalling left of a coastal point, a gage at the point will see

    a. high waters before landfall
    b. high waters after landfall

2. For storms landfalling right of a coastal point, a gage at the point will see

    a. low waters before landfall
    b. low waters after landfall
    c. an excursion immediately after landfall due to a splitting of waves under the core of high waters; this profile is highly idealized and rarely occurs in nature so precisely.

Storms produce a local, quasi-steady state, dynamic surge situation on the coast prior to storm arrival. These are sometimes called "precursors" or "forerunners", that is, the first or earliest tail end of profiles given in figure C1. With arrival of the storm, the state is then superseded or wiped

out by a new, rapidly changing, dynamic situation. After storm passage, a quasi-steady state, dynamic situation reforms. For an along-shore moving storm the two quasi-steady states are in opposite sense; whereas, for a track perpendicular to the coast, they are similar, see figure C1.

One can begin computations with an initially quiescent sea, and the storm at a set distance from shore; if larger storm distances from shore (longer computer runs) do not appreciably change the computed coastal surge during the active time of the coastal surge, then initialization is optimized. The SPLASH models operate with this technique for shelf surges. If the storm is initialized too close to shore, there will be over and undershoots of surge on the coast with time; if farther from the coast, the over and undershoots are reduced; farther distances have little effect on the computed coastal surge and this is wasteful of computer resources. In this situation, the forerunners (if present, and not laced with wave set-up) are in general quickly computed by the model since they are a temporary, quasi-steady-state phenomena. Now, if the real sea has a pre-determined sea level anomaly, then it should be added onto the computed coastal surge or else the datum of the basin changed accordingly.

On a shelf, the coastal surge response from driving forces may be quick and hence insensitive to initial storm placement if set sufficiently far from shore. Inside a bay, however, the response may be slower and more sensitive to initial storm position because it takes time for waters to move into or out of a bay.

Sometimes bay models initialize with a quiescent bay and "initial set-up" on the ocean side of the bay; sometimes "initial set-up" is used inside the entire bay as well as the ocean side. One must be careful here to test for sensitivities of surges inside the bay, especially if the storm is arbitrarily initialized on the shelf and close to the bay. When calibrating a bay model, one should not merely add on some biased positive set-up (unless it is an anomaly); if such is required to aid calibration, the model may have shortcomings. When calibrating a model with a given historical storm it should be ascertained that the final results are insensitive to storm induced initial set-up and initial storm placement; e.g., empirical tests made with the storm placed further away from the bay and initial set-up* changed accordingly.

In calibrated bay models, empirical tests should be made to determine optimum, initial storm distance from shore. The optimum distance, however, may be very distant from shore (much further than a shelf model) if the model starts with a quiescent sea. For convenience, models sometimes are initialized with a pre-arranged, storm-induced, initial height inside the bay and the storm close to shore. The validity or accuracy of this approach should be tested. This can be done by setting the initial storm position further from shore, setting a concomitant smaller initial water height inside the bay, and then comparing final computed surge heights for separate runs; if the final surge heights do not change significantly, the model is optimized for initialization.

---

* The computed surge output from a shelf model, initialized with a quiescent sea, may not be appropriate as input boundary conditions for a bay model; e.g., the response of a bay has a different sensitivity to initialization than shelf models.

C. Some Comments on Storm Models and Driving Forces in Basins

Some storm surge models ignore the pressure gradient force of a storm and substitute instead a static-inverted-barometer effect. This can be a mistake because the dynamic effects from a moving pressure gradient force across the sea surface can substantially exceed the static effect.

Some older surge models employ empirical or simple storm models to generate driving forces. This can be dangerous if the storm model is designed to generate forces acting on small scale items such as buildings. Storm models should be designed for generation of long gravity or shallow water waves on the continental shelf. These waves are sensitive to storm characteristics which may be poorly specified in empirical or simple storm models.

Many storm models compute wind for a circularly-symmetric, stationary storm on one ray from the storm center, and the winds are assumed parallel to the concentric isobars or else angled off by some empirical amount; storm motion effects then may or may not be incorporated.

Many storm models use an analytic pressure profile as input to a wind formulation, but the direction of the wind is not accounted for. A common pressure formulation is

$$\frac{P - P_o}{\Delta P} = e^{-R/r} \tag{1}$$

where $\Delta P = P_{oo} - P_o$, P_{oo} is ambient pressure surrounding the storm, P_o is the storm's central pressure, and R is a space parameter (usually the distance from storm center to maximum winds). When fitting eq. (1) to real data there are problems. Usually, the fitting is forced to agree about the core of the storm for a given P_o; in this case, P_{oo} is left to wander on its own without any control, sometimes to unrealistic values.

There is also a fitting problem with R for wind formulations when using eq. (1). To show this, consider cyclostrophic wind:

$$W_c^2 = \frac{r}{\rho} \frac{dP}{dr} \tag{2}$$

When eq. (1) is plugged into eq. (2), the maximum wind $(W_c)_{max}$ occurs at r = R. Now consider the geostrophic wind:

$$W_{geo} = \frac{1}{\rho f} \frac{dP}{dr} \tag{3}$$

where f is the coriolis parameter. When eq. (1) is plugged into eq. (3), the maximum wind $(W_{geo})_{max}$ occurs at r = R/2. If a gradient wind formulation is used, then the maximum wind $(W_{grad})_{max}$ occurs between R/2 and R. Usually for tropical storms, the maximum wind occurs near the position of the maximum cyclostrophic wind; the discrepancy of the computed storm size and R is magnified as the storm increases in size and pressure drop becomes smaller.

If an observed storm size is substituted for R in eq. (1), then the computed position of the maximum gradient wind from the storm center will be smaller than the input parameter R.

If a gradient wind formulation, through eq. (1), is used, then it must be fitted to measured wind data at a given altitude for the effects of friction; the gradient wind profile is usually fitted by scaling with a best fit constant. Before such a wind model is accepted in a surge model, it should be tested for sensitivities; by sensitivities the writer means testing the output-computed-surge with the surge model for a range of inflow angles of the wind, other fittings of the pressure profile to control P_{oo} to realistic values, R scaled properly to reflect actual storm size, a range of scaled constant for the effects of friction, and the effects of storm motion on the wind. Even though the surge and storm models are calibrated for a one storm situation with the computed surge comparing near perfect with observed data, this in itself may not be sufficient. What is desirable is a universal calibration of the surge and storm models for a range of real storm situations, a range of real basins, and real surge data. Calibration in a universal sense has been discussed previously.

To compute surges with a dynamic surge model, it is helpful if the storm model is dynamically consistent on the sea surface. By dynamically consistent the writer means equations of motion are satisfied so that pressure, wind and inflow angle (wind direction across isobars) are in balance. With this balance, certain errors in meteorology can be tolerated. In fact, the storm model can be designed without maximum wind as input data; this is desirable because observed winds have a noisy structure, are not generally observed on the sea surface, the average sampling time is not clearly specified, the maximum wind is hard to define, and small errors in wind produce large errors in surges (for all scale sizes* the same, the surge varies as the wind squared). On the other hand, central pressure, or pressure drop of the storm, is desirable as input data because it is relatively easy to measure on the sea surface, has a much less noisy structure than wind, and small errors produce only small errors in storm surge (for all scale sizes* the same, the surge varies almost linearly with pressure, Jelesnianski 1972).

As an example of the usefullness of a dynamically consistent storm model, consider a fixed pressure drop. An error or change in storm size will change the wind and hence the surge; however, the inflow angle will also change (in opposite sense to the wind change) and hence the surge. These two separate changes oppose each other in surge generation and the coastal surge heights, when normalized with respect to storm size, are then quasi-conservative with respect to changes in storm size. In any case, the peak surge is quasi-conservative to errors in wind, when compensated by biased errors in inflow

---

* For constant storm size, an increase in wind implies an increase in pressure drop. Also, the inflow angle changes and this is of some consequence in surge generation.

angle. Of course the errors do not oppose exactly in a one-to-one manner and one or the other may dominate depending on scale size; with changing storm size in a given basin, the dynamics of surge generation also changes. An important thing to realize is that surges are not monotonic with respect to any one storm parameter, such as maximum winds, because of the resulting action from other parameters; unexpected reversals in surge amplitude can occur with changes in storm parameters.

A dynamically consistent storm model on the sea surface does not mean surge amplitudes are computed properly or accurately; it is difficult to design an adequate storm model to represent nature. It means however, that the dynamics of surge generation are better portrayed and critical situations and reversal of surge amplitude can be better specified. Also, the sensitivities of surge generation inherent with an empirical storm model are reduced.

Sometimes storm models are designed to decrease winds in bays, estuaries, and near shore regions because of frictional effects from the neighboring land. Physically the decrease may be true, but it does not automatically follow that the generated surge will be smaller than those with uncorrected ocean winds. Any local decrease in wind may be associated with larger inflow angle, and the drag coefficient of the wind may also be larger. These feedback effects are, of course, masked in calibration procedures; for, if the model winds are too strong or weak, then the calibration coefficients of the surge model will adjust accordingly. However, it is not wise to calibrate for situations with, say, uncorrected winds and then for different situations to apply the same calibration coefficients with corrected winds. The physics for the storm model input data, and the equations of motion, should be consistent in production runs to those of the calibration procedure.

If one computes surges with a dynamic surge model, the model storm should have dynamic sophistication equivalent to the ocenographic surge model; an exception are bays for which surge generation may be dominated by input boundary conditions--but even so, the storm model used in a shelf-surge model must properly generate input boundary conditions that are coupled with bay and shelf models.

For operational use such as forecasting and planning, a poorly designed storm model may prove an exercise in futility and it would be better then to explore surge phenomena by statistical rather than dynamic techniques.

D. Some Comments on Short Gravity-Wind Waves and Wave Set-up

Short gravity wind waves are generated by a storm. The periods are measured in seconds and the lengths in fraction of a kilometer. The storm creates many wind waves; whereas, the long gravity surge wave is a single forced wave which may or may not be attended with a few long gravity-wave resurgences or free waves. Because of small differences in period and length of seperate wind waves, they can superimpose at times to form an extraordinary high amplitude. Near the coast, they are akin to wave trains and ride atop the long gravity-wave surge. Short gravity-wind waves generally break offshore with only residual effects on the coastal amplitude of the storm surge; however, there are occasions when the effects are substantial compared to the storm surge. The long gravity-wave storm surge does not produce a long breaker,

but under appropriate conditions will cascade energy into short waves over an area small compared to its length; these will mix with the wind waves and break.

When wind waves travel across a sloping beach toward shore, there is an induced change of the still water surface called "wave set-up", figure C2. The induced wave set-up is roughly the mean water height relative to a hypothetical still-water level in the absence of wind waves. The passing wave train has an envelope of high waters or crests, an envelope of low waters or troughs, and in between a wave set-up, surface envelope that does not agree with the still water line in the absence of waves. It is difficult to isolate the wave set-up and crest height from tide gage readings, or from high water marks in buildings, except under controlled laboratory experiments. The wave set-up is variable; it is negative seaward of breaking wave activity (a set-down slope), positive landward of breaking wave activity (a set-up slope).

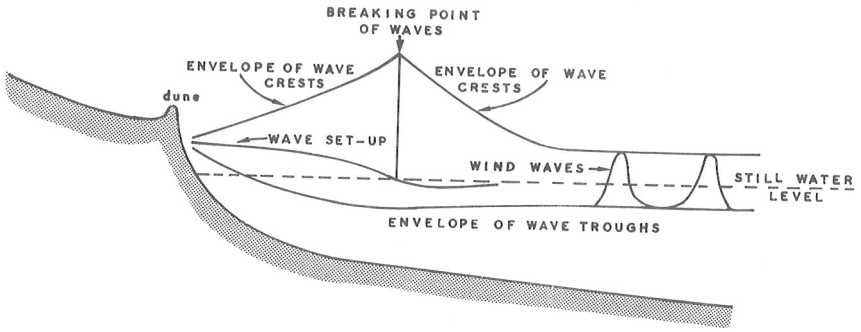

Figure C2.--Idealized, one-dimensional schemata of wave envelopes and wave set-up in the near shore region. The juncture of the three solid lines on the coast is imprecise because of run-up and backwash from the breaking waves. If the dune is overtopped by the still water level (storm surge), then the surge waters can penetrate miles inland on low terrain; the major effects from the breaking waves are limited to the near shore region.

Wave set-up depends on the character of the wind wave, the breaking character, the on-offshore coastal depth profile, and position along the depth profile relative to the breaking wave position; hence, for a variety of storms and storm tracks, wave set-up is difficult to ascertain in any local region. The treatment of wave set-up in a surge model is almost an art based on the expertise of the modeler. It can be made implicit in the calibration procedure.

Occasionally, particularly large amplitude wind waves will ride atop a large amplitude storm surge in shelf areas with deep waters just off the coast. In this situation, the waves will break close to shore or even inland because of inland inundation from the storm surge and the deep offshore waters. If buildings are located between the dune and shore (less than a few hundred ft. from the coast) and in the regime between wave set-up and wave crest, figure C2, than this is a particularly dangerous predicament during a storm surge. In this situation the waters in the buildings may have, in addition to wave set-up, a capricious add-on accumulation of water that can be significantly higher than the still-water-level storm surge; this is due to periodic run-

up inundation from the remnants of breaking waves entering upper level openings (doors, cracks, windows, etc.). Tide gages, however, do not have upper level openings and the smoothed readings are relatively insensitive to the periodic wave phenomena, except for wave set-up.

A building's interior acts as a stilling well, just as a tide gage, and presumably has equivalent wave set-up. The add-on accumulation of water in buildings (if any) from upper level openings is one reason why high water marks in the edifices are occasionally higher than measurements from a nearby tide gage; similarly, why neighboring buildings with different upper level openings record different high water marks. Also, some buildings are tightly constructed and it is then more difficult for water to enter.

The SPLASH model was calibrated with data from tide gages and measured high water marks. These contain wave set-up in a random fashion because the geographical location of the data points relative to the origin of breaking wave location is unknown. In the data sample, no attempt was made to discriminate wave set-up from the storm surge. No dynamic refinement was made for severe wave set-up or isolated wave set-up to depend on the storm, shore geometry, and inland distance from shore. As a result, the calibration loosely implies wave set-up in a statistical sense and without regard to any dynamical considerations. This means severe wave set-up is underforecast, weak wave set-up is overforecast. Similarly for the action of waters between the wave set-up and crest, figure C2.

The surge forecaster should be aware that wave set-up and add-on accumulations in buildings are generally limited to the landward nearshore region between the dune and coast (several hundred ft) whereas if the still-water storm surge level overtops the dune then waters from the surge can penetrate miles inland on low and flat terrain. Breaking wave activity and wave set-up may be more pronounced on the landward nearshore regions when deep waters are just off the coast; some examples are the Pensacola-Panama City coast and Ft. Lauderdale-Vero Beach coast. If the waves break inland, the wave set-up may be small but the direct action of the waves themselves can be very destructive. If waters are shallow just off the coast, and if the on-offshore beach slope is small, then breaking wave phenomena is at some distance from the coast with only residual effects inland from the coast.

(Continued from inside front cover)

WBTM TDL 25 Charts Giving Station Precipitation in the Plateau States From 850- and 500-Millibar Lows During Winter. August F. Korte, Donald L. Jorgensen, and William H. Klein, September 1969. (PB-187-476)

WBTM TDL 26 Computer Forecasts of Maximum and Minimum Surface Temperatures. William H. Klein, Frank Lewis, and George P. Casely, October 1969. (PB-189-105)

WBTM TDL 27 An Operational Method for Objectively Forecasting Probability of Precipitation. Harry R. Glahn and Dale A. Lowry, October 1969. (PB-188-660)

WBTM TDL 28 Techniques for Forecasting Low Water Occurrences at Baltimore and Norfolk. James M. McClelland, March 1970. (PB-191-744)

WBTM TDL 29 A Method for Predicting Surface Winds. Harry R. Glahn, March 1970. (PB-191-745)

WBTM TDL 30 Summary of Selected Reference Material on the Oceanographic Phenomena of Tides, Storm Surges, Waves, and Breakers. N. Arthur Pore, May 1970. (PB-192-449)

WBTM TDL 31 Persistence of Precipitation at 108 Cities in the Conterminous United States. Donald L. Jorgensen and William H. Klein, May 1970. (PB-193-599)

WBTM TDL 32 Computer-Produced Worded Forecasts. Harry R. Glahn, June 1970. (PB-194-262)

WBTM TDL 33 Calculation of Precipitable Water. L. P. Harrison, June 1970. (PB-193-600)

WBTM TDL 34 An Objective Method for Forecasting Winds Over Lake Erie and Lake Ontario. Celso S. Barrientos, August 1970. (PB-194-586)

WBTM TDL 35 Probabilistic Prediction in Meteorology: a Bibliography. Allan H. Murphy and Roger A. Allen, June 1970. (PB-194-415)

WBTM TDL 36 Current High Altitude Observations--Investigation and Possible Improvement. M. A. Alaka and R. C. Elvander, July 1970. (COM-71-00003)

NOAA Technical Memoranda

NWS TDL-37 Prediction of Surface Dew Point Temperatures. R. C. Elvander, February 1971. (COM-71-00253)

NWS TDL-38 Objectively Computed Surface Diagnostic Fields. Robert J. Bermowitz, February 1971. (COM-71-00301)

NWS TDS-39 Computer Prediction of Precipitation Probability for 108 Cities in the United States. William H. Klein, February 1971. (COM-71-00249)

NWS TDL-40 Wave Climatology for the Great Lakes. N. A. Pore, J. M. McClelland, C. S. Barrientos, and W. E. Kennedy, February 1971. (COM-71-00368)

NWS TDL-41 Twice-Daily Mean Monthly Heights in the Troposphere Over North America and Vicinity. August F. Korte, June 1971. (COM-71-00826)

NWS TDL-42 Some Experiments With a Fine-Mesh 500-Millibar Barotropic Model. Robert J. Bermowitz, August 1971. (COM-71-00958)

NWS TDL-43 Air-Sea Energy Exchange in Lagrangian Temperature and Dew Point Forecasts. Ronald M. Reap, October 1971. (COM-71-01112)

NWS TDL-44 Use of Surface Observations in Boundary-Layer Analysis. H. Michael Mogil and William D. Bonner, March 1972. (COM-72-10641)

NWS TDL-45 The Use of Model Output Statistics (MOS) To Estimate Daily Maximum Temperatures. John R. Annett, Harry R. Glahn, and Dale A. Lowry, March 1972. (COM-72-10753)

NWS TDL-46 SPLASH (Special Program To List Amplitudes of Surges From Hurricanes) I. Landfall Storms. Chester P. Jelesnianski, April 1972. (COM-72-10807)

NWS TDL-47 Mean Diurnal and Monthly Height Changes in the Troposphere Over North America and Vicinity. August F. Korte and DeVer Colson, August 1972. (COM-72-11132)

NWS TDL-48 Synoptic Climatological Studies of Precipitation in the Plateau States From 850-, 700-, and 500-Millibar Lows During Spring. August F. Korte, Donald L. Jorgensen, and William H. Klein, August 1972. (COM-73-10069)

NWS TDL-49 Synoptic Climatological Studies of Precipitation in the Plateau States From 850-Millibar Lows During Fall. August F. Korte and DeVer Colson, August 1972. (COM-74-10464)

NWS TDL-50 Forecasting Extratropical Storm Surges For the Northeast Coast of the United States. N. Arthur Pore, William S. Richardson, and Herman P. Perrotti, January 1974. (COM-74-10719)

NWS TDL-51 Predicting the Conditional Probability of Frozen Precipitation. Harry R. Glahn and Joseph R. Bocchieri, March 1974. (COM-74-10909/AS)

NWS TDL-52 SPLASH (Special Program to List Amplitudes of Surges From Hurricanes) II. General Track and Variant Storm Conditions. Chester P. Jelesnianski, March 1974.

NWS TDL-53 A Comparison Between the Single Station and Generalized Operator Techniques for Automated Prediction of Precipitation Probability. Joseph R. Bocchieri, September 1974. (COM-74-11763/AS)

NWS TDL-54 Climatology of Lake Erie Storm Surges at Buffalo and Toledo. N. Arthur Pore, Herman P. Perrotti, and William S. Richardson, December 1974.

NWS TDL-55 Dissipation, Dispersion and Difference Schemes. Paul E. Long, Jr., May 1975. (COM-75-10972/AS)

NWS TDL-56 Some Physical and Numerical Aspects of Boundary Layer Modeling. Paul E. Long, Jr., May 1975. (COM-75-10980)

NWS TDL-57 A Predictive Boundary Layer Model. Wilson A. Shaffer and Paul E. Long, Jr., May 1975.

NWS TDL-58 A Preliminary View of Storm Surges Before and After Storm Modifications for Alongshore-Moving Storms. Chester P. Jelesnianski and Celso S. Barrientos, October 1975. (PB247362)

NWS TDL-59 Assimilation of Surface, Upper Air, and Grid-Point Data in the Objective Analysis Procedure for a Three-Dimensional Trajectory Model. Ronald M. Reap, February 1976.

NWS TDL-60 Verification of Severe Local Storm Warnings Based on Radar Echo Characteristics. Donald Foster, June 1976.

NOAA--S/T 76-2259